eLife

Reviewed Preprint
v1 • November 18, 2025
Not revised

Reviewed Preprint
v2 • July 21, 2026
Revised by authors

Targeting tankyrase scaffolding in the β-catenin destruction complex by PROTAC overcomes the limitation of catalytic inhibitors in cancer

Qian Wang[1], Liping Li[1], Lin You[1], Shuai Wang[1], Lei Han[1], Bingnan Wang[1], Liping Yao[1], Yesu Addepalli[1], Yong Lu[1], Ilgen Mender[2], Ann M Flusche[2], Chiho Kim[1,3], Nageswari Yarravarapu[2], Andrew Lemoff[1], Lawrence Lum[2,*], Jerry W Shay[2], Yonghao Yu[1,3], Chuo Chen[1]

[1]Department of Biochemistry, UT Southwestern Medical Center, Dallas, United States • [2]Department of Cell Biology, UT Southwestern Medical Center, Dallas, United States • [3]Department of Molecular Pharmacology and Therapeutics, Columbia University Vagelos College of Physicians and Surgeons, New York, United States

For correspondence: Chuo.Chen@UTSouthwestern.edu

* Present address: Apertor Pharmaceuticals, South San Francisco, United States

Competing interests: No competing interests declared

Funding: See page 31

Reviewing editor: Roel Nusse, Stanford University, United States

eLife Assessment

This **important** study reports the development of the first tankyrase degrader and demonstrates its enhanced ability to inhibit β-catenin signaling compared to conventional tankyrase inhibitors. The evidence supporting the conclusions is comprehensive and **convincing**, based on rigorous biochemical and cellular analyses. The findings will be of broad interest to researchers studying Wnt signaling, protein degradation, and cancer biology.

https://doi.org/10.7554/eLife.109052.2.sa5

Abstract

Aberrant WNT/β-catenin signaling drives tumorigenesis and metastasis in cancer. Although enzymatic inhibitors of tankyrase (TNKS) effectively block AXIN degradation and stabilize the β-catenin destruction complex (DC), they have demonstrated limited efficacy in various cancer models. Here we demonstrate that, unexpectedly, the induction of AXIN puncta represents a major barrier to achieving therapeutic efficacy. Mechanistically, catalytic inhibition of TNKS prevents TNKS turnover and drives its accumulation in the DC, wherein the scaffolding function of TNKS induces AXIN puncta formation, rigidifies the DC, and impedes β-catenin turnover. Chemically induced degradation of TNKS overcomes this limitation by stabilizing AXIN without puncta formation, providing a deeper suppression of the WNT/β-catenin pathway activity and the proliferation of colorectal cancer cells harboring dysfunctional APC mutations. Collectively, these findings provide an explanation for the unsatisfactory outcomes of drugging the WNT/β-catenin signaling pathway by TNKS inhibitors and highlight TNKS degradation as a promising approach to treat WNT/β-catenin-driven cancers.

Introduction

WNT/β-catenin signaling plays an important role in cell growth, differentiation, and migration[1,2]. Dysregulation of this pathway enables reprogrammed cancer cells to proliferate, metastasize and resist chemo- and radiotherapies. In colorectal cancer (CRC), loss-of-function mutations in adenomatous polyposis coli (APC) are the major drivers of aberrant WNT/β-catenin signaling[3]. However, therapeutic targeting this oncogenic pathway remains unsuccessful despite extensive efforts[4]. For example, although silencing tankyrase (TNKS1/2, also known as PARP5A/B and ATRD5/6)[5–7] phenocopied APC restoration and prevented tumorigenesis in *APC*-null mice[8], TNKS

inhibitors (TNKSi) failed to show promising efficacy in various in vitro and in vivo CRC models. Addressing the discrepancy between the genetic and pharmacological interception of WNT/β-catenin signaling through TNKS may provide a path toward developing new CRC treatments.

The axis inhibition protein (AXIN) and APC are both scaffolding proteins of the β-catenin destruction complex (DC) that exists as biomolecular condensates in the cytoplasm to prime β-catenin for proteasomal degradation[9–11]. As TNKS-catalyzed poly(ADP-ribose)-dependent ubiquitination (PARdU) is required for the turnover of AXIN[12–14], blocking the enzymatic function of TNKS by IWR1 or XAV939 leads to AXIN accumulation[12,15], thereby enhancing the ability of the DC to promote β-catenin degradation. The accompanied AXIN puncta formation is generally attributed to AXIN accumulation and is considered to play a positive role in suppressing WNT/β-catenin signaling. However, TNKS also associates with the DC[16–18], where its contributions to the DC function remains poorly understood.

Specifically, because TNKS regulates its own abundance through self-poly(ADP-ribosylation) (PARylation), catalytic inhibition also promotes drastic TNKS accumulation[12]. It is unclear whether this feedback mechanism affects the DC function and results in the limited anticancer efficacy of TNKSi, as inhibitor-induced TNKS accumulation may support WNT/β-catenin signaling through molecular scaffolding independently of its catalytic function. Indeed, deletion of the catalytic PARP domain of TNKS attenuated, but did not fully suppress the WNT-induced transcription of the TCF/LEF-controlled genes[12,16,19]. By contrast, removal of the sterile alpha motif (SAM) domain or the ankyrin repeat clusters (ARCs) of TNKS abolished the WNT/β-catenin pathway activity more completely.

To understand the role of TNKS scaffolding in WNT/β-catenin signaling, we developed a TNKS-targeting proteolysis-targeting chimera (PROTAC)[20,21] as a selective TNKS degrader (TNKSd). Comparison between TNKSd and TNKSi allowed us to understand the catalysis-independent scaffolding function of TNKS and uncover the mechanism underlying the ineffectiveness of TNKSi against cancers. We found that inhibiting TNKS by TNKSi led to the accumulation of TNKS within the DC, which induced AXIN puncta formation, promoted maturation[22,23] of the DC condensates, and impeded β-catenin turnover. In contrast, degrading TNKS by TNKSd enriched AXIN without inducing puncta or impairing the dynamics of the DC. As a result, TNKSd provided deeper suppression of the WNT/β-catenin pathway activity as well as better control of the proliferation of CRC cells harboring dysfunctional APC mutations. Collectively, our study provides new insights into the roles of TNKS in the DC and presents a promising strategy to enhance the therapeutic efficacy of TNKS-targeting anticancer treatments.

Results

IWR1-POMA induces TNKS degradation

To study the role of TNKS scaffolding, we first developed a PROTAC molecule to enable selective degradation of TNKS1 and TNKS2 at the same time by small molecules. Compared to conventional genetic approaches, this chemical approach helps address gene redundancy more conveniently and effectively. TNKS uses nicotinamide adenine dinucleotide (NAD^+) as the ADP-ribose donor. The corresponding pocket in the PARP domain contains two discrete sites, one for nicotinamide (NI) and the other for adenosine (AD) binding. IWR1 is a highly selective TNKSi that exploits the AD site unique to TNKS, and IWR6 is a promiscuous but potent TNKSi structurally similar to XAV939 that binds to the NI site common to all PARPs[12,24]. Based on the crystal structures of TNKS1 and TNKS2 in complex with IWR1 or XAV939 (Figure S1), we envisioned that modifying the quinoline group of IWR1 and the phenyl group of IWR6 would not negatively impact TNKS-binding. We have thus created a small library of 30 PROTAC molecules by attaching pomalidomide[25] or VH032[26] through a PEG chain of various lengths to IWR1 or IWR6 (Figure S2A) for engaging cereblon (CRBN) or the von HippelLJLindau tumor suppressor protein (VHL), respectively, and examined their ability to induce TNKS degradation.

To facilitate the discovery of a TNKSd, we also developed a luciferase assay to measure the level of TNKS1 in a high-throughput manner. Using the CRISPR-assisted insertion tagging (CRISPaint) technology[27], we introduced a nanoluciferase (NanoLuc) tag to the C-terminus of TNKS1 in HAP1 cells (Figure S2B). We chose to monitor TNKS1 because it is constitutively expressed while TNKS2 is expressed minimally under basal conditions. By following the luciferase activity, the knockdown efficiency of all 5 series of the PROTAC molecules could be quantified easily and accurately using a robotic liquid dispenser system in 96-well plates, which significantly improved the efficiency over the traditional method that relies on Western blotting and image processing. Using this luciferase assay, we found that the IWR1-based PROTACs eliminated TNKS1 significantly more effectively than the IWR6-based PROTACs (Figure S2C). Additionally, CRBN mediated TNKS1 degradation more efficiently than VHL. Inserting a triazole group between the quinoline group and the PEG chain further enhanced the degradation efficiency. However, replacing the PEG linker with a nonpolar or rigid linker did not improve the efficacy, and employing G007-LK[28] as the warhead with various linker strategies led to reduced potency and degree of degradation (Figure S2D).

IWR1-TP4-Poma (IWR1-POMA hereafter) is the most potent PROTAC among these series. It initiated TNKS1 degradation at 1 nM, operated with a DC_{50} value of 60 nM, and reached 96% degradation at 1.2 μM in HAP1 cells (Figure 1A). Western blot analysis confirmed that IWR1-POMA could also deplete TNKS1 and suppress the induction of TNKS2 in a dose and time-dependent manner in DLD-1 CRC cells that carry truncating APC mutations (Figure 1B and C). The level of TNKS did not recover 36 hours after IWR1-POMA was removed, indicating a durable drug effect (Figure S3A). Addition of IWR1, pomalidomide, or MG132 blocked TNKS degradation (Figure S3B and C), supporting that IWR1-POMA functioned through the designed mode of action. The generality of IWR1-POMA to induce TNKS degradation was demonstrated in SW480, HT-29 and HeLa cells (Figure S3D). The ability of IWR1-POMA to stabilize AXIN and promote β-catenin degradation in the cytoplasm was confirmed further in HEK293 cells (Figure 1D). Compared to IWR1, IWR1-POMA provided better control of the cytosolic β-catenin level. The performance of this PROTAC molecule is particularly notable, considering that shutting down the catalysis of TNKS leads to a >30-fold accumulation of total TNKS, creating a nearly 3-orders-of-magnitude difference in the levels of TNKS between catalytic inhibition and chemically induced degradation. Although hook effect was observed at high concentrations, presumably due to the formation of nonproductive binary protein-ligand complexes under these conditions, to our knowledge, this is the first example of targeted degradation of an auto-regulated protein.

To confirm the ability of IWR1-POMA to engage TNKS, we prepared IWR1-PEG3-NCT as a bioluminescence resonance energy transfer (BRET) tracer (Figure S3E)[29]. We then treated HAP1-TNKS1-NanoLuc cells with MG132 to increase the signal-to-noise ratio and to normalize the TNKS level in the presence of IWR1 and IWR1-POMA. Addition of IWR1 effectively reduced the BRET signals; however, the intrinsic fluorescence[30] of IWR1-POMA prevented the assessment of its binding affinity by this method. Nonetheless, the observation of significant BRET signals of IWR1-POMA at high concentrations prompted us to test whether it could be used directly as a BRET acceptor for NanoLuc despite poor spectral overlap[31]. Indeed, the BRET signals increased in a dose-dependent manner after adding IWR1-POMA to HAP1-TNKS1-NanoLuc cells in the presence of MG132 (Figure S3F). Accordingly, we titrated IWR1 into HAP1-TNKS1-NanoLuc cell in the presence of 0.5 μM of IWR1-POMA and found that IWR1 suppressed the BRET signals with an IC_{50} value of 0.25 μM (Figure S3G). Repeating this experiment in 293T cells transfected with TNKS1-NanoLuc plasmid improved the BRET signal-to-noise ratio and confirmed that the pomalidomide chromophore can be used as a BRET pair for NanoLuc. It also confirmed that IWR1-POMA (0.5 μM) binds to TNKS1 with a slight reduction in affinity as compared to IWR1 (IC_{50} 0.15 μM).

To examine the degradation specificity of IWR1-POMA, we performed proteome-wide expression profiling on DLD-1 cells treated with DMSO, IWR1 or IWR1-POMA for 16 h. Using a tandem mass tag (TMT)-based, multiplexed quantitative mass spectrometric (MS) approach with two biologically independent replicate samples (Figure S4A), we identified 7,884 proteins, among which 5,822 could be quantified with high confidence (<1% FDR). Correlation analysis confirmed the

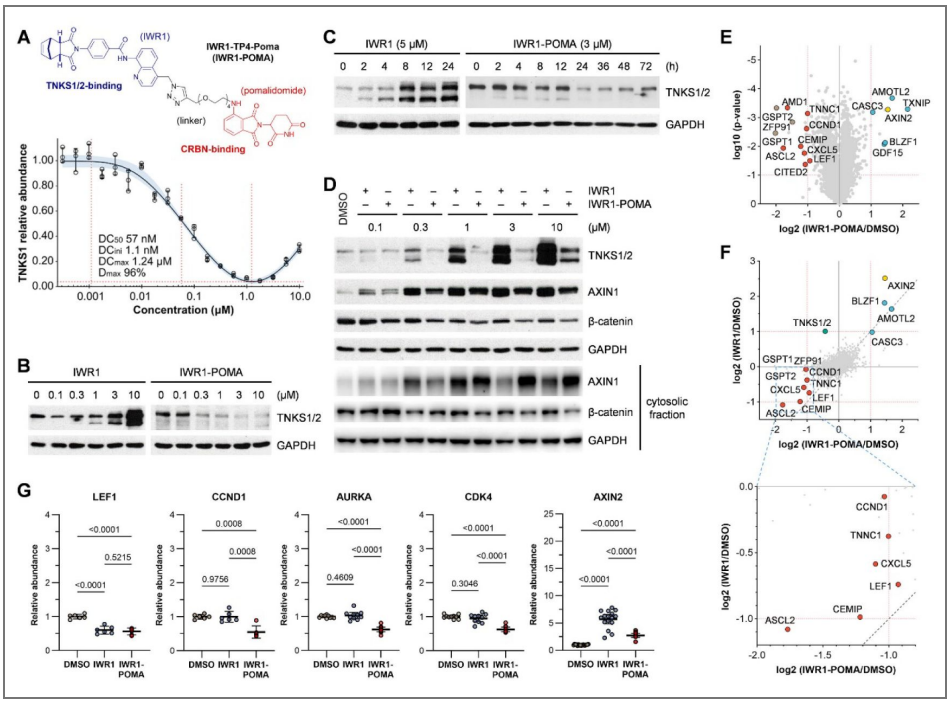

Figure 1. Characterization of IWR1-POMA

(A) IWR1-POMA induced TNKS degradation with a DC_{50} value of 60 nM and reached a nearly complete depletion of TNKS1 at 1.2 μM in HAP1 cells. The dose-response curve is presented as mean ± SEM (n = 3 biological samples) with 95% confidence interval (CI) indicated by the shaded area. (B and C) IWR1 induced massive TNKS accumulation while IWR1-POMA promoted deep degradation in a dose and time-dependent manner in DLD-1 cells. (D) IWR1-POMA promoted a more complete degradation of β-catenin than IWR1 in HEK293 cells cultured with Wnt3A conditioned media. (E) Volcano plot of the TMT experiment results. TNKS substrates (light blue) accumulated and WNT/β-catenin-regulated proteins (red) downregulated in DLD-1 cells treated with IWR1-POMA (3 μM). AXIN2 (yellow) is both a TNKS substrate and a WNT target. GSPT1/2 and ZFP91 (light brown) are the only off-targets identified. (F) Comparative analysis of the TMT experiment showing that the levels of several WNT/β-catenin regulated proteins (red) were preferentially reduced by IWR1-POMA relatively to IWR1 treatment. The dashed line denotes equal protein abundance between the two treatments. Data points above this line in Quadrant III represent proteins selectively downregulated by IWR1-POMA relatively to IWR1. (G) Relative peptide abundances of selected WNT targets in the TMT experiment with p-values calculated by two-tailed unpaired t-test.

consistency of the quantitative analysis of the two biological replicates (Figure S4B). However, accurate quantification of TNKS1 proved challenging, as only a low-abundance peptide corresponding to TNKS1 was detected in this experiment. Nonetheless, IWR1-POMA induced the accumulation of AXIN2 along with other TNKS substrates (Figure 1E). LEF1 and several other WNT targets were also effectively downregulated, confirming the on-target drug effects. Pairwise binary comparison of the drug treatment versus control indicated better control of WNT signaling by IWR1-POMA in addition to high degradation specificity (Figure 1F and G). GSPT1/2 and ZFP91, three common off-targets of the IMiD-based PROTACs, were the only perturbations not related to the WNT pathway. None of the other 7 PARPs and 81 NAD^+/$NADP^+$-dependent enzymes identified in this MS experiment were significantly affected by IWR1-POMA (Figure S4C).

PROTAC suppresses catalysis-independent WNT/β-catenin signaling by TNKS

A previous study showed that polymerization of PARylation-incompetent TNKS can drive WNT/β-catenin signaling[19]. To understand whether the lack of efficacy of TNKSi in suppressing CRC cell growth originated from the PARylation-independent WNT/β-catenin signaling induced by the accumulated TNKS upon catalytic inhibition, we treated Wnt3A-stimulated 293T cells with IWR1 or IWR1-POMA. We reason that, by removing both the catalysis-dependent and independent functions of TNKS, IWR1-POMA may suppress WNT/β-catenin signaling more completely than IWR1 that inhibits AXIN PARylation but also promotes TNKS accumulation and polymerization. Indeed, IWR1-POMA promoted β-catenin degradation significantly more effectively than IWR1 under various doses of Wnt3A (Figure S5A). To investigate the individual contribution of TNKS1 and TNKS2 to WNT/β-catenin signaling, we co-transfected a low dose of TNKS1 plasmid together with SuperTopFlash (STF), a luciferase reporter for the WNT/β-catenin activity, into 293T-TNKS1/2-DKO cells wherein both TNKS1 and TNKS2 were deleted by CRISPR[32] (Figure S5B). We found that addition of IWR1 suppressed the TNKS1-induced STF activity but not completely (Figure 2A and S5C). There was a small but noticeable residual activity, which could not be removed by increasing the concentration of IWR1. In contrast, IWR1-POMA induced TNKS1 degradation and promoted deeper suppression of the STF activity. Similarly, IWR1-POMA reduced the level of TNKS2 and provided better control of the STF activity than IWR1 in TNKS1/2-DKO cells expressing TNKS2 (Figure 2B and S5D). As such, both TNKS1 and TNKS2 can contribute to WNT signaling that persists even in the presence of catalytic inhibition of TNKS PARylation.

We next used PARylation-incompetent variants of TNKS to verify whether TNKS1 and TNKS2 can promote WNT/β-catenin signaling independently of their catalytic function. The catalytic site of TNKS is highly conserved. Deactivation of the H-Y-E triad of TNKS1 with H1184A and E1291A mutations[33] abolishes the binding of NAD^+ and the accepting ADP ribose. This PARP-dead (PD) variant induced notable WNT/β-catenin signaling in the TNKS1/2-DKO cells even at low doses, confirming that TNKS1 has a catalysis-independent functional role in the DC (Figure 2C and S5E). Addition of IWR1-POMA degraded TNKS1-PD and reduced the pathway activity, whereas treatment with IWR1 had no effect. Similarly, TNKS2-M1054V having an impaired ability to interact with the accepting ADP ribose[34] induced robust WNT/β-catenin signaling and was insensitive to IWR1 treatment (Figure 2D and S5F). In contrast, IWR1-POMA degraded this catalytically inactive variant of TNKS2 and suppressed the corresponding STF activity in a dose-dependent manner. Collectively, these data support the hypothesis that both TNKS1 and TNKS2 play an additional role in the DC to regulate WNT/β-catenin signaling through a mechanism beyond catalytic PARylation of AXIN[19]. Degradation of TNKS eliminates both the enzymatic and non-enzymatic activities of TNKS, providing better control of the WNT/β-catenin signaling than catalytic inhibition (Figure S5G).

Tankyrase controls the dynamic assembly of the DC

AXIN interacts with APC to work as a molecular scaffold for the DC to catalyze β-catenin phosphorylation and ubiquitination. TNKS also associates with this complex[16–18] to control the AXIN level. Although much is known about the catalytic function of TNKS, its scaffolding

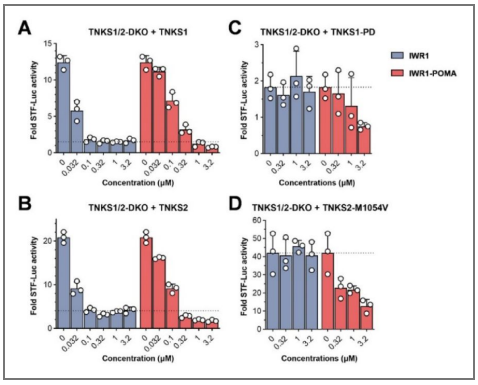

Figure 2. IWR1-POMA degraded TNKS to suppress both catalysis-dependent and independent WNT signaling

(A) 293T-TNKS1/2-DKO cells were transfected with FLAG-TNKS1 and STF plasmids and then treated with IWR1 or IWR1-POMA. In contrast to IWR1 that plateaued in suppressing the WNT/β-catenin signaling induced by TNKS1, IWR1-POMA allowed for a more complete control of the pathway activity. (B) 293T-TNKS1/2-DKO cells transfected with FLAG-TNKS2 and STF plasmids and then treated with IWR1 or IWR1-POMA similarly showed that catalytic inhibition led to residual WNT/β-catenin activity. (C) 293T-TNKS1/2-DKO cells were transfected with 3×FLAG-TNKS1-PD and STF plasmids and then treated with IWR1 or IWR1-POMA. IWR1-POMA suppressed the luciferase activities whereas IWR1 had no effect. (D) 293T-TNKS1/2-DKO cells transfected with FLAG-TNKS2-M1054V and STF plasmids and then treated with IWR1 or IWR1-POMA. TNKS2 exhibited robust scaffolding effects. All data are presented as mean ± SEM (n = 3 biological samples).

function[19,35] is poorly understood. To study the non-enzymatic function of TNKS in WNT signaling, we transfected 293T cells with a low dose of AXIN1-mCherry plasmid and confirmed that TNKS colocalized with AXIN1 to form micrometer-sized puncta (Figure 3A and S6). In contrast, in TNKS1/2-DKO cells that lack TNKS, AXIN1-mCherry distributed diffusely throughout the cytoplasm as small aggregates (Figure 3B). However, AXIN puncta formed readily when AXIN1-mCherry was expressed together with TNKS1 in the TNKS1/2-DKO cells (Figure 3C). Similarly, TNKS2 also induced AXIN puncta in TNKS1/2-DKO cells (Figure 3D), suggesting that TNKS1 and TNKS2 play a redundant structural role in the DC to support AXIN puncta formation. To further verify whether AXIN PARylation is involved in the puncta formation, we expressed AXIN1-mCherry together with catalytically inactive variants of TNKS and found that both TNKS1-PD and TNKS2-M1054V could induce AXIN puncta effectively (Figure 3E and F). Quantitative imaging analysis confirmed that TNKS1 and TNKS2 promoted AXIN puncta formation through molecular scaffolding independently of their ability to catalyze protein PARylation (Figure 3G).

Both IWR1 and IWR1-POMA stabilize AXIN to suppress WNT/β-catenin signaling. However, IWR1 induces TNKS accumulation while IWR1-POMA promotes TNKS degradation. Given the observation that AXIN puncta formation requires TNKS, we next examined how these TNKS modulators affect the assembly of the DC. As expected, treating SW480 cells with IWR1 induced AXIN puncta while IWR1-POMA did not (Figure 4A and B). Similarly, IWR1 induced AXIN puncta in 293T cells wherein the endogenous AXIN1 was labeled with RFP at its C-terminus by CRISPR[36], but IWR1-POMA failed to induce AXIN puncta (Figure 4C and D). As 293T cells harbor wild-type APC and SW480 cells carry a truncating APC without the AXIN-binding sites[37,38], the ability of TNKSi to induce AXIN puncta is independent of AXIN-APC binding. These results also suggest that tagging AXIN1 with a fluorescent protein does not affect its ability to oligomerize.

To further understand the functional significance of AXIN puncta, we transfected HeLa cells with a low dose of AXIN1-GFP plasmid. Again, IWR1 promoted the formation of micrometer-sized AXIN puncta that are significantly larger than those observed in the DMSO control sample (Figure 4E and F). In contrast, AXIN1 distributed diffusely throughout the cytoplasm when the cells were treated with IWR1-POMA. To determine the effects of AXIN puncta on WNT signaling, we expressed AXIN1-GFP together with STF in HeLa cells under the same conditions and found that IWR1-POMA suppressed the luciferase activity better than IWR1 (Figure 4G). Thus, AXIN puncta formation is not a prerequisite for the DC to catalyze β-catenin degradation as commonly believed. Instead, the large AXIN puncta induced by IWR1 are less functional DCs than the unaggregated AXIN complexes formed upon IWR1-POMA treatment. We have further confirmed that the N-terminally tagged AXIN1 and the C-terminally tagged AXIN2 also responded to IWR1 and IWR1-POMA treatments in the same manner (Figure S7C and D).

The DC is a classic example of biomolecular condensates[9,10]. TNKS interact with both AXIN and APC and can self-aggregate to form insoluble filaments[17,34,35,39,40]. We suspected that the massive accumulation of TNKS induced by IWR1 rigidified the DC[22,23] and limited its ability to turn over β-catenin. To test this hypothesis, we expressed AXIN1-mCherry and mNeonGreen-β-catenin in HeLa cells and then treated these cells with DMSO, IWR1 or IWR1-POMA. AXIN1-mCherry and mNeonGreen-β-catenin colocalized in all samples, indicating that labeling AXIN1 and β-catenin with a fluorescent protein did not disrupt the recruitment of β-catenin to the DC (Figure 5A). We then performed fluorescence recovery after photobleaching (FRAP) analysis on AXIN1-mCherry to investigate the structural role of TNKS in the DC. After photobleaching, the fluorescence signals of the AXIN-mCherry puncta in the DMSO control samples recovered quickly (k = 0.093 s^{-1}, n = 21), indicating a dynamic assembly of the DC (Figure 5B)[41,42]. However, the fluorescence signals of the AXIN1-mCherry puncta in the IWR1-treated sample recovered slowly (k = 0.036 s^{-1}, n = 16) and plateaued at 62% level, in contrast to 78% for the DMSO control, suggesting that IWR1 rigidified the DC. In contrast, the dynamics of the fluorescence recovery of the few very small AXIN1-mCherry puncta in the IWR1-POMA-treated sample was comparable to that of the DMSO control (k = 0.090 s^{-1}, 71% recovery, n = 21). Because both IWR1 and IWR1-POMA stabilized AXIN (Figure 5C), the rigidification of the DC by IWR1 is not a result of AXIN accumulation. Instead, as the DC puncta in the IWR1-treated sample was enriched with and that in the IWR1-POMA-treated sample

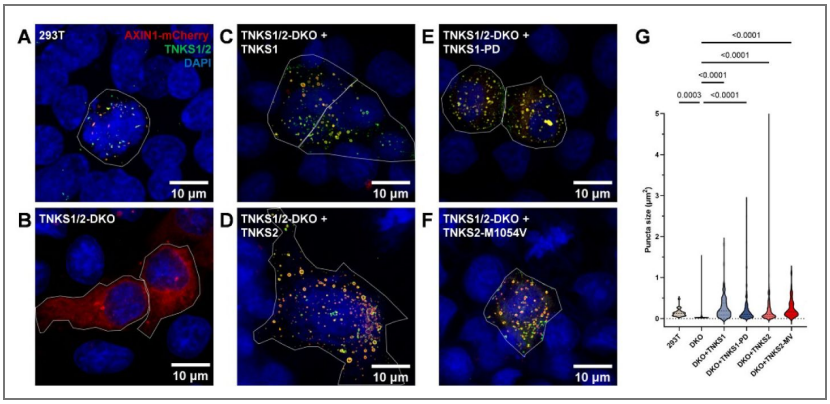

Figure 3. TNKS is required for AXIN puncta formation

(A) AXIN colocalized with TNKS and formed puncta in 293T cells transfected with AXIN1-mCherry plasmid. (B) AXIN distributed diffusely throughout the cytoplasm in TNKS1/2-DKO cells transfected with AXIN1-mCherry plasmid. (C) Introduction of TNKS1 restored AXIN puncta in TNKS1/2-DKO cells transfected with AXIN1-mCherry and TNKS1 plasmids. (D) TNKS2 also induced puncta formation in TNKS1/2-DKO cells transfected with AXIN1-mCherry and TNKS2 plasmids.(E) The catalytic function of TNKS1 is not required for puncta formation as demonstrated in TNKS1/2-DKO cells transfected with AXIN1-mCherry and TNKS1-PD plasmids. (F) Catalytically inactive TNKS2-M1054V also promoted AXIN puncta formation effectively in TNKS1/2-DKO cells transfected with AXIN1-mCherry and TNKS2-M1054V plasmids. (G) Quantification of the AXIN1-mCherry puncta in 293T cells (n = 28 biological samples), TNKS1/2-DKO cells (n = 230 biological samples), TNKS1/2-DKO cells in the presence of TNKS1 (n = 115 biological samples), TNKS1/2-DKO cells in the presence of TNKS2 (n = 229 biological samples), TNKS1/2-DKO cells in the presence of TNKS1-PD (n = 246 biological samples), and TNKS1/2-DKO cells in the presence of TNKS2-M1054V (n = 86 biological samples). Data are presented with p-values calculated by two-tailed unpaired t-test.

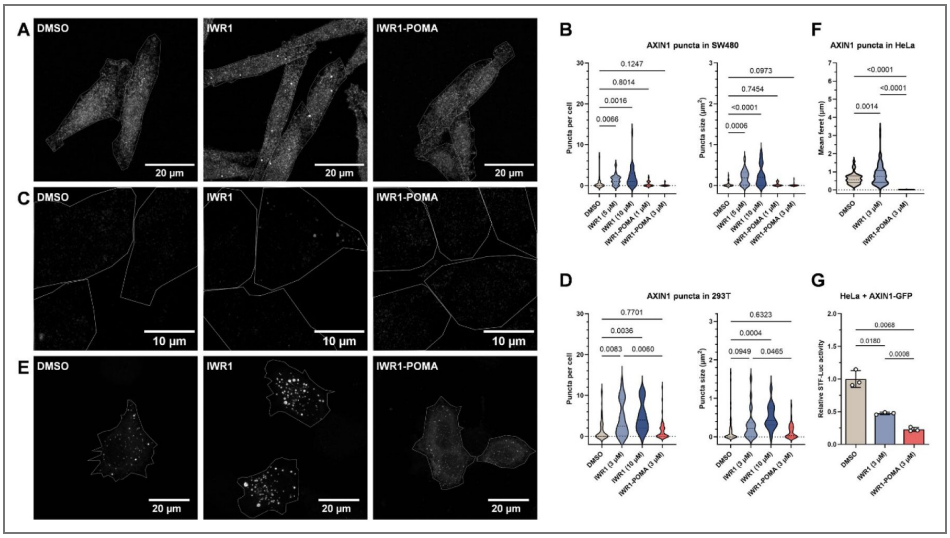

Figure 4. Chemically induced TNKS accumulation promoted AXIN puncta formation

(A) SW480 cells treated with DMSO, IWR1 (5 μM), or IWR1-POMA (1 μM) and stained with anti-AXIN1 antibody. (B) Numbers and sizes of the AXIN puncta in SW480 cells treated with DMSO (n = 36 biological samples), IWR1 (5 μM, n = 20 biological samples, or 10 μM, n = 31 biological samples), or IWR1-POMA (1 μM, n = 17 biological samples, or 3 μM, n= 24 biological samples) for 16 h. (C) 293T-AXIN1-dsRed-KI cells treated with DMSO, IWR1 (3 μM), or IWR1-POMA (3 μM). (D) Numbers and sizes of the AXIN puncta in 293T-AXIN1-dsRed-KI cells treated with DMSO (n = 82 biological samples), IWR1 (3 μM, n = 39 biological samples, or 10 μM, n = 32 biological samples), or IWR1-POMA (3 μM, n= 61 biological samples) for 16 h. (E) HeLa cells were transfected with AXIN1-GFP plasmid and then treated with DMSO, IWR1 (3 μM), or IWR1-POMA (3 μM). IWR1 promoted the formation of micrometer-sized AXIN puncta whereas IWR1-POMA dissolved them. (F) Numbers and sizes of the AXIN1 puncta in HeLa cells transfected with AXIN1-GFP plasmide and treated with DMSO (n = 88 biological samples), IWR1 (3 μM, n = 91 biological samples), or IWR1-POMA (3 μM, n = 151 biological samples) for 16 h. (G) HeLa cells transfected with AXIN1-GFP and STF plasmids and then treated with DMSO, IWR1 (3 μM) or IWR1-POMA (3 μM). IWR1-POMA suppressed WNT/β-catenin signaling significantly better than IWR1, indicating that AXIN puncta formation is not required for the DC to promote β-catenin degradation. Data are presented as mean ± SEM (n = 3 biological samples) with p-values calculated by two-tailed unpaired t-test for all data.

depleted with TNKS, the reduction of the DC dynamics by IWR1 most likely originated from TNKS accumulation. We next performed FRAP analysis on mNeonGreen-β-catenin to examine the functional role of TNKS scaffolding in the DC using the dynamics of β-catenin as a measurement for its turnover rate (k = 0.024 s^{-1}, 78% recovery, n = 11 for the DMSO control). In contrast to IWR1-POMA that accelerated the fluorescence recovery of mNeonGreen-β-catenin (k = 0.046 s^{-1}, 76% recovery, n = 10), IWR1 reduced the level of recovery by 20% without affecting the kinetics (k = 0.028 s^{-1}, 58% recovery, n = 16). These results suggest that TNKSi functions in part through cytosolic retention of β-catenin, and TNKS accumulation negatively impacts the exchange of β-catenin in the DC (Figure 5D). Collectively, our data support the hypothesis that TNKS scaffolding augments AXIN puncta to limit the ability of the DC to effectively degrade β-catenin.

Tankyrase degradation prevents CRC cell proliferation

Loss of functional APC impairs the DC function and results in constitutive WNT/β-catenin signaling that drives tumorigenesis and metastasis of CRC. Whereas depletion of both TNKS1 and TNKS2 by shRNA phenocopied APC restoration to prevent tumorigenesis in mice[8,43], TNKSi only showed modest anti-proliferative activities in a limited number of CRC cell lines[44]. For example, IWR1 had minimal effects on the proliferation of DLD-1 cells that express truncated forms of APC. Remarkably, IWR1-POMA was able to suppress the formation of DLD-1 cell colonies under both normal and low serum conditions (Figure 6A and S8A). Similarly, the proliferation of SW480 and HT-29 cells carrying different truncating APC mutations were also better suppressed by IWR1-POMA (Figure 6A and S8B). The anti-proliferative activity also correlated with the ability of IWR1-POMA to better suppress WNT/β-catenin signaling in DLD-1 and SW480 cells (Figure S8C). Mechanistically, several WNT-controlled genes showed differential responses to IWR1 and IWR1-POMA. For example, whereas LEF1 was downregulated in both IWR1 and IWR1-POMA treated samples, cyclin D1 and Aurora kinase A responded to IWR1-POMA only in DLD-1 cells (Figure 1F and G and S8D). This observation is consistent with the ability of IWR1-POMA to better inhibit WNT/β-catenin signaling. Interestingly, IWR1-POMA also reduced the level of CDK4 while IWR1 had no effect, which may be explained by CDK4 being a direct target of c-MYC that in turn is a direct target of WNT/β-catenin. Indeed, IWR1-POMA reduced the level of c-MYC while IWR1 did not (Figure S8D). Taken together, targeted degradation of TNKS offers better control of the WNT/β-catenin pathway activities important to the maintenance of CRC cells than catalytic inhibition.

GSPT1, a translation termination factor that binds eRF1 to mediate translation termination, is frequently identified as a neosubstrate of CRBN in the presence of the IMiD class of small molecules[45]. For example, targeting GSPT1 for degradation by CC-90009 (eragidomide) perturbs the global proteome, activates the integrated stress response (ISR) and induces apoptosis in acute leukemia (AML) cells[46,47]. However, the observation that the VHL-based PROTACs could also induce TNKS1 degradation (Figure S2C) and the addition of IWR1 readily abolished the ability of IWR1-POMA to degrade TNKS (Figure S3C) suggest that IWR1-POMA did not deplete TNKS through affecting translation termination globally.

Several lines of evidence further support that the observed growth inhibition by IWR1-POMA is a result of on-target degradation of TNKS. First, HCT116 cells harboring a mutation in one β-catenin allele that cannot be phosphorylated by the DC showed remarkable resistance to IWR1-POMA (Figure 6B and S9A). Second, IWR1-POMA had no effect on the level of cytosolic β-catenin in 293T-TNKS1/2-DKO cells that lack both TNKS1 and TNKS2 (Figure S9B), indicating that IWR1-POMA downregulated β-catenin in a TNKS-dependent manner. Third, the GSPT1/2 degrader CC-90009 had no effect on TNKS and the cytosolic β-catenin levels in DLD-1 cells (Figure S9C). Fourth, we have further exposed DLD-1 cells to CC-90009 and established resistant cells (DLD-1R) that lacked the expression of GSPT1/2 (Figure S9D). TNKS in DLD-1R remained responsive to IWR1 and IWR1-POMA treatments (Figure S9E), and IWR1-POMA was still able to prevent the proliferation of DLD-1R cells effectively (Figure 6B and S9F). As such, IWR1-POMA suppressed WNT-dependent cancer cell proliferation through degrading TNKS but not GSPT1/2. However, consistent with catalytic inhibition or knocking down both TNKS1 and TNKS2 stabilized PTEN and suppressed the growth of RKO cells[48], IWR1-POMA also suppressed the proliferation of RKO cells

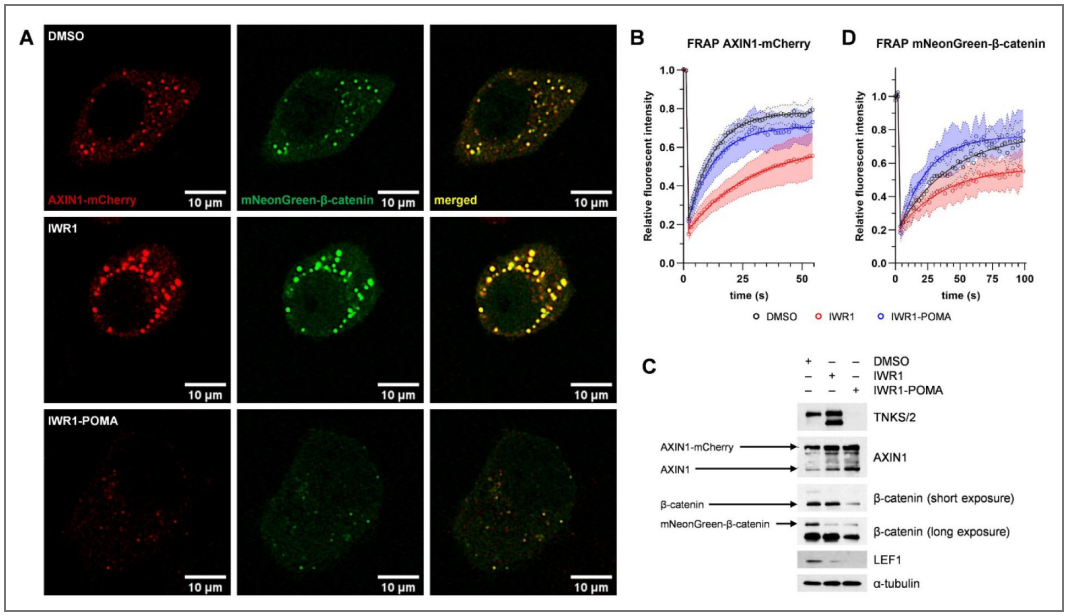

Figure 5. TNKS accumulation impeded the degradation of β-catenin

(A) HeLa cells were transfected with AXIN1-mCherry and mNeonGreen-β-catenin plasmids and then treated with DMSO, IWR1 (3 μM) or IWR1-POMA (3 μM). IWR1 promoted large AXIN1 puncta formation and IWR1-POMA dissolved the puncta. β-Catenin colocalized with AXIN1, indicating the proper assembly of the DC. (B) FRAP analysis provided support to the hypothesis that TNKS controls the dynamic assembly of the DCs. IWR1 treatment led to a slow recovery of the AXIN1-mCherry fluorescent signal after photobleaching. In contrast, IWR1-POMA treatment did not affect the mobility of AXIN1. The fluorescent recovery curves were fitted to one-phase association model. Data are presented as mean with 95% CI. (C) Western blot analysis of samples corresponding to Figure 5A confirmed the accumulation of TNKS by IWR1 and the depletion TNKS by IWR1-POMA. The deeper suppression of the Wnt/β-catenin signaling by IWR1-POMA is also supported by the reduced levels of total β-catenin. (D) FRAP analysis indicated that IWR1 limited the turnover of β-catenin. In contrast, IWR1-POMA accelerated the diffusion rate of β-catenin in the DC. The fluorescent recovery curves were fitted to one-phase association model. Data are presented as mean with 95% CI.

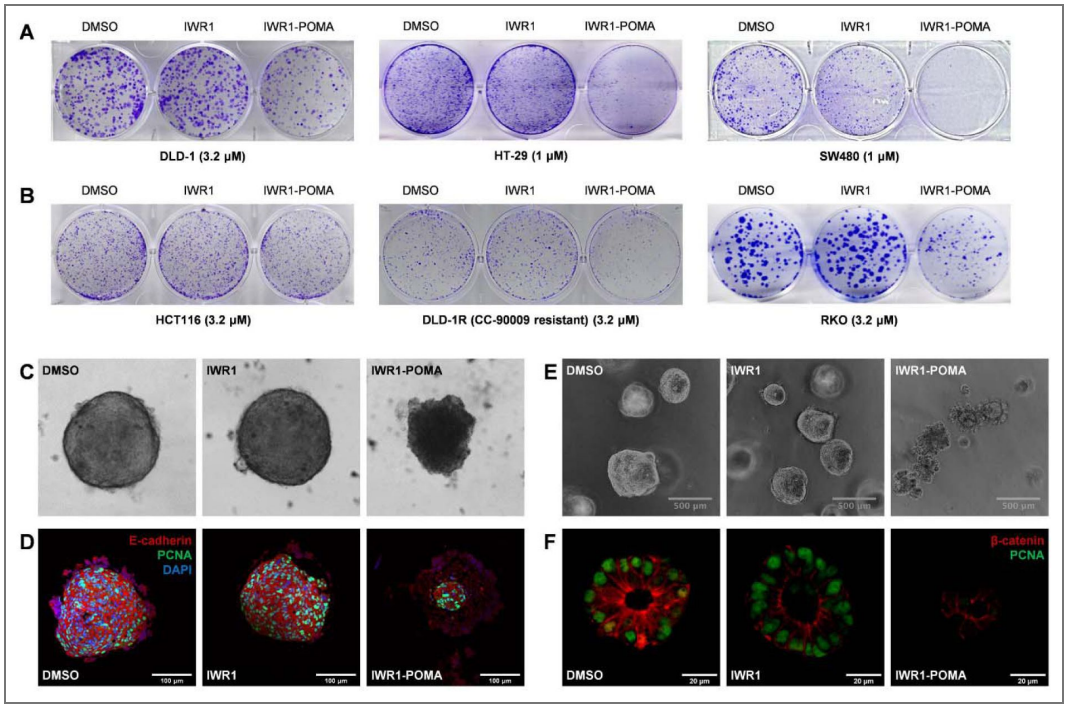

Figure 6. **IWR1-POMA suppressed CRC cell growth**

(A) IWR1-POMA suppressed the formation of DLD-1, SW480, and HT-29 CRC colonies significantly more effectively than IWR1. (B) HCT116 cells carrying a mutation in β-catenin that could not be processed by the DC were resistant to both IWR1 and IWR1-POMA. Additionally, DLD-1R cells obtained from cultivating DLD-1 cells with the GSPT1/2 inhibitor CC-90009 were still sensitive to IWR1-POMA treatment. IWR1-POMA could also inhibit RKO cells carrying full-length APC through the PTEN-AKT axis. (C) DLD-1 cells were developed into 3D spheroids and then treated with DMSO, IWR1 (5 μM), or IWR1-POMA (5 μM) for 10 d. The spheroids treated with IWR1-POMA lost the tight, spherical structure while IWR1 had no effect. (D) Immunostaining showed that the DLD-1 spheroids treated with IWR1-POMA only contained a small core of living cells while those treated with IWR1 remained highly proliferative. (E) IWR1-POMA (1 μM) suppressed the growth of PDM-7 patient-derived CRC organoids of approximately 200 μm in diameter with an apoptotic phenotype while IWR1 (1 μM) had no effect. (F) IWR1-POMA (1 μM) reduced the level of β-catenin and suppressed the proliferation of PDM-7 organoids grown from single cells significantly more effectively than IWR1 (1 μM).

that carry full-length APC (Figure 6B and S9G). This result indicates that targeting TNKS by IWR1-POMA can also suppress cancer cell growth through the PTEN-AKT axis independently of the WNT/β-catenin pathway.

To investigate the anticancer potential of IWR1-POMA further, we used DLD-1 and SW480 cells to establish 3D spheroids that recapitulated the cell-cell interactions and the hypoxia core of tumors. Consistent with colony formation assays, IWR1 had no effect on the size and the morphology of these spheroids, while IWR1-POMA suppressed their growth effectively (Figure 6C and S10A). Notably, the outer layer of the spheroids treated by IWR1-POMA had a loose structure incapable of supporting a spherical shape. Instead, they adapted a rather flat architecture with a small core of aggregated cells. Immunostaining showed that the outer layer of these IWR1-POMA-treated spheroids did not contain living cells (Figure 6D). The presence of significant DNA breaks in this region (Figure S10B) is consistent with the observation that APC restoration induced apoptosis in CRC cells[49].

We have also evaluated the anticancer effects of IWR1-POMA in a human CRC organoid model that preserved the multicellular identity of the tumor more faithfully than immortalized cancer cells. The PDM-7 patient-derived primary CRC cells harbor truncating mutations in APC, making it susceptible to WNT inhibition. We first confirmed that the PDM-7 organoids maintained the heterogeneous nature of the proliferation and the WNT activity within the organoids (Figure S10C). We next confirmed that IWR1-POMA could prevent the formation of PDM-7 organoids whereas IWR1 had little or no effect (Figure S10D). We then treated established PDM-7 organoids with IWR1 or IWR1-POMA and found that, in contrast to IWR1 that did not affect their growth, IWR1-POMA inhibited the proliferation of these organoids with an apoptotic phenotype (Figure 6E and S10E and F) and promoted β-catenin degradation more effectively than IWR1 (Figure 6D). Collectively, removing TNKS scaffolding is important for achieving anticancer efficacy in CRC by targeting TNKS.

Discussion

In the existing model of WNT/β-catenin signaling, AXIN is a key component of the DC. It interacts with APC to work as a scaffolding protein for the DC to catalyze β-catenin phosphorylation and ubiquitination. In the cytoplasm, TNKS also associates with the DC and controls the AXIN level through PARdU[12–14]. As such, AXIN accumulates upon TNKS inhibition, leading to enhanced β-catenin degradation and reduced WNT/β-catenin pathway activities[12,15]. Traditionally, the formation of AXIN puncta is viewed as a hallmark of functional DC induction[16–18], wherein the increased local concentration of DC components enhances its "effective activity"[50,51]. Because TNKS inhibition induces large AXIN puncta, it is generally believed that TNKSi supports the formation of highly functional DCs to accelerate the turnover of β-catenin. However, given the newly discovered role of TNKS scaffolding[19,35], the mechanism by which TNKS controls WNT signaling needs refinement. In this study, we show that AXIN puncta formation relies on the scaffolding but not the catalytic function of TNKS, which is consistent with the previous report that knocking down both TNKS1 and TNKS2 prevented G007-LK to induce AXIN puncta in SW480 cells[18]. However, the function role of TNKS scaffolding in the DC remained unaddressed. Interestingly, blocking proteasomal degradation by MG132 promoted TNKS accumulation but the resulting DC exhibited a different phenotype as compared to that induced by G007-LK[18]. It is likely that the PAR chains helped suppress TNKS aggregation as observed with PARP1.

The DC is a classic example of biomolecular condensates[9,10]. It containing tens to hundreds of AXIN and APC molecules in a ~1:1 ratio to catalyze β-catenin degradation[50]. Both AXIN and APC contain extensive intrinsically disordered regions, which are likely important for providing a flexible structure to support catalysis. TNKS interacts with AXIN and APC through multivalent binding in the DC. Based on this work, the catalysis-independent function of TNKS in WNT/β-catenin signaling originates from its ability to promote maturation[22,23] of the DC condensates. Specifically, because TNKS aggregates and forms filaments at high concentrations[34,39,40], large AXIN puncta containing excess TNKS are rigid and exhibit reduced catalytic activity. In contrast, in the absence of TNKS, the small AXIN complexes are dynamic and catalyze β-catenin degradation

more effectively. As such, the size of the AXIN complex does not inform the activity of the DC. This notion is consistent with the previous observation that AXIN2 can also support β-catenin degradation despite having a reduced ability to form puncta[52]. Collectively, our study suggests that TNKS controls WNT/β-catenin signaling through two independent mechanisms: it regulates AXIN homeostasis through catalytic PARylation[12]; meanwhile it dictates the material properties of the DC through molecular scaffolding. The mechanism by which TNKS antagonizes the DC through molecular scaffolding is also reminiscent of the effect of disheveled (DVL) polymerization on the WNT/β-catenin signalosome[53].

The development of TNKSi as an anticancer drug has been discouraged by the lack of significant efficacy in various in vitro and in vivo models. Our data suggest that TNKSd can overcome this limitation by stabilizing AXIN without affecting the DC dynamics. Therefore, TNKSd can provide better suppression of the WNT/β-catenin-controlled genes important for cancer cell proliferation than TNKSi. In particular, we identify several WNT target genes that are suppressed by TNKSd but not TNKSi. Among them, Aurora A is an oncogene frequently amplified in CRC[54]. Because Aurora A binds to and stabilizes c-MYC that is also dysregulated in many cancers[55], the ability of IWR1-POMA to downregulate both c-MYC and Aurora A more effectively than IWR1 likely contributed to its improved anti-proliferative activity. Another WNT/β-catenin downstream target specifically regulated by TNKSd is cyclin D1. The CDK4/cyclin D1 complex is a key regulator of cell cycle, and CDK4 blockade has been explored as a potential strategy to enhance the anticancer efficacy of TNKSi[56,57]. Interestingly, TNKSd, but not TNKSi, also downregulated CDK4 expression potentially through c-MYC. We speculate that the coordinated action of IWR1-POMA on CDK4 and cyclin D1 additionally contributed to its improved anticancer efficacy. Finally, TNKSi can sensitize cancer cells toward EGFR or MEK inhibition[58,59]. As a more effective suppressor of Wnt/β-catenin signaling, IWR1-POMA may provide a better therapeutic window for treating cancers driven by WNT/β-catenin signaling using a corresponding combinatorial approach.

Some previous studies showed that TNKSi induced reversible intestinal toxicity at high doses without significant antitumor effects in mice[28,60]. However, others found that suppressing the proliferation of *Lgr5*$^{+}$ intestinal stem cells by TNKSi did not affect the morphology of the tissue or cause weight loss[61–63], and the selective TNKS inhibitor basroparib was well tolerated in a recently disclosed Phase 1 clinical study[64]. As constitutive silencing of TNKS in *APC*-null mice prevented tumorigenesis without damaging the intestines[8], the observed on-target toxicity of TNKSi may associate with TNKS accumulation at high doses, akin to the cytotoxicity induced by PARP1-trapping upon catalytic inhibition, and reverse allostery[65] in TNKS has been proposed[40]. Studying TNKS complexes in normal tissues under these conditions may help delineate the source of intestinal toxicity. Finally, targeting the TNKS ARC or SAM domains offers an alternative approach to suppress WNT/β-catenin signaling without promoting TNKS oligomerization[66,67]. Targeting the ARC may further differentiate the WNT-dependent and independent activities of TNKS and provide finer resolution in TNKS inhibition. We are thus cautiously optimistic for continued investment in aggregation-free TNKS-targeting in CRC.

Materials and Methods

Cell lines

HAP1, DLD1, HEK293, 239T, HeLa, HT-29, SW480, RKO, and L-Wnt3A cells obtained from Horizon Discovery or ATCC were cultured according to the vendors' recommended procedures. L-Wnt3A cells were used to generate conditioned medium following the protocol described by Nusse (*https://wnt.stanford.edu/purification%23old#medium*). PDM-7 obtained from ATCC were grown into organoid according to the procedures provided by ATCC using the Organoid Growth Kit 1A and cell basement membrane for organoid culture from ATCC.

CRISPR engineering of HAP1 cells

HAP1 cells were transiently transfected with pCRISPaint-NanoLuc-PuroR and pCAS9-mCherry-Frame+2 plasmids and a TNKS1 sgRNA plasmid targeting 5'-TCACTAGGTCTTCTGCTCTGCGG-3' and selected by puromycin treatment. Cells were then cultured in 96 well plates to generate single colonies and sequenced to select for correct incorporation of nanoluciferase at the C-terminus of TNKS1.

DLD-1R cells

DLD-1 cells were cultivated with an increasing concentration of CC-90009 (0.1, 1 and 10 μM) to confer resistance to GSPT inhibition. Western analysis confirmed the loss of GSPT1 expression in these cells. GSPT2 is a low-abundance protein in DLD-1 and DLD-1R not detectable by Western blot, which is consistent with a reported quantitative proteomic analysis of DLD-1 cells (GSPT1: 102,567 ppb, GSPT2: 2,495 ppb; *https://www.ebi.ac.uk/gxa/experiments/E-PROT-18/Results*)[68].

Determination of TNKS degradation

HAP1-TNKS1-NanoLuc cells at 30LJ50% confluence were treated with different concentrations of PROTAC molecules in triplicates for 16 h. The TNKS1 level was quantified by QUANTI-Luc Gold (Invivogen) with normalization to the total protein content. For high-throughput screens, the cells were seeded into 96-well plates at 2×10^4 cells per well with 100 μL culture media. The PROTAC molecules dissolved in DMSO were placed in T8+ dispensehead cassettes and then introduced by the TECAN D300e Digital Dispenser with series dilutions under the D300e software control. To determine the DC_{50} value of IWR1-POMA, the dose-response relationship was fitted to a Bayesian Gaussian Processes model in R using code developed by Semenova[69].

Immunoblot assays

Cells were washed once with cold PBS and lysed with the SDS lysis buffer (1% SDS, 10 mM HEPES, pH 7.0, 2 mM $MgCl_2$ and 500LJU universal nuclease). Subcellular protein fractions were obtained by using the Mem-PER Plus Kit (Thermo Fisher Scientific). Briefly, the cell pellets were suspended in the cell permeabilization buffer with cOmplete EDTA-free protease inhibitor cocktail (Sigma) and incubated for 15 min at 4 °C followed by centrifugation at 16,000 × *g* for 15 min to provide the cytosolic fraction. The pellets were then suspended in the cell permeabilization buffer with 0.5% NP-40 and protease inhibitors, passed through a 27½-gauge needle for 30 times, and centrifuge at 16,000 × *g* for 15 min to give the cytosolic fraction, and the pellets were suspended in RIPA buffer with protease inhibitors with sonication to provide the nuclear fraction. Alternatively, cells were incubated in eight volumes of hypotonic buffer (20 mM HEPES-KOH, pH 7.9; 10 mM KCl; 2 mM $MgCl_2$; 0.3% NP-40; 1 mM DTT; 1 mM EDTA; and 1× protease inhibitor cocktail) on ice for 20 min and then centrifuged at 3,000 × *g* for 10 min at 4°C to provide the cytosolic extracts. Protein concentrations were determined by the BCA assay kit (Thermo Fisher Scientific). A total of 20 μg of proteins were loaded onto the SDS–PAGE gel and then transferred to a nitrocellulose membrane. Nitrocellulose membranes were then blocked with Tris buffered saline containing 0.1% Tween-20 and 5% milk (Bio-Rad). Membranes were incubated with the primary antibodies overnight at 4LJ°C and then the secondary antibodies for 1LJh at room temperature. The blots were developed with or without enhanced chemiluminescence and were exposed on autoradiograph films or imaged by a BioRad Molecular Imager ChemiDoc XRS System.

Quantitative mass spectrometry

DLD-1 cells at 40% confluence were treated with the drug for 24 h, washed with cold PBS and lysed with the SDS lysis buffer. Protein concentrations were determined by the BCA assay kit (Thermo Fisher Scientific). Two biological replicate samples were prepared with 500 μg of proteins from each sample, reduced with 2 mM DTT for 10 min and alkylated with 50 mM iodoacetamide for 30 min in dark, and then extracted using methanol-chloroform precipitation. The protein pellets were dissolved in 400 μL 8 M urea buffer (8 M urea, 50 mM Tris-HCl, 10 mM EDTA, pH 7.5) and digested

by Lys-C (Wako, at a 1:100 enzyme/protein ratio) for 2 h. The urea concentration was then reduced to 2 M using freshly made 100 mM ammonium bicarbonate solution. Proteins were subsequently digested with trypsin (Thermo Fisher Scientific, at 1:100 enzyme/protein ratio) overnight. Peptides were desalted with Oasis HLB cartridges (Waters) and re-suspended in 200 mM HEPES (pH 8.5) to a final concentration of 1 μg/μL. For each sample, 100 μg of peptides were reacted with the corresponding amine-based TMT reagents (Thermo Fisher Scientific) for 1 h. The reactions were quenched with 5% hydroxylamine solution and were combined. Samples were then desalted and a reverse-phase fractionation spin column (Pierce) was used according to the manufacturer's directions to fractionate the sample into 8 fractions. The fractions were dried in a SpeedVac and reconstituted in a 2% acetonitrile, 0.1% TFA buffer followed by injecting onto an Orbitrap Fusion Lumos mass spectrometer coupled to an Ultimate 3000 RSLC-Nano liquid chromatography system. Samples were injected onto a 75 μm×75-cm EasySpray column (Thermo) and eluted with a gradient from 0→28% buffer B over 180 min. Buffer A contained 2% (v/v) acetonitrile and 0.1% formic acid in water, and buffer B contained 80% (v/v) acetonitrile, 10% (v/v) trifluoroethanol, and 0.1% formic acid in water. The mass spectrometer operated in positive ion mode with a source voltage of 1.8 kV and an ion transfer tube temperature of 275 °C. MS scans were acquired at 120,000 resolution in the Orbitrap and top speed mode was used for SPS-MS3 analysis with a cycle time of 2.5 s. MS2 was performed with CID with a collision energy of 35%. The top 10 fragments were selected for MS3 fragmentation using HCD, with a collision energy of 55%. Dynamic exclusion was set for 25 s after an ion was selected for fragmentation. The raw MS data files were analyzed using Proteome Discoverer v2.4 (Thermo), with peptide identification performed using Sequest HT searching against the human protein database from UniProt. Fragment and precursor tolerances of 10 ppm and 0.6 Da were specified, and three missed cleavages were allowed. Carbamidomethylation of Cys and TMT10plex labelling of N-termini and Lys side-chains were set as fixed modifications, with oxidation of Met set as a variable modification. Protein abundances were determined based on the sum of the signal-to-noise ratios of the reporter ions for all peptides matched to each protein. The false-discovery rate (FDR) cutoff was 1% for all peptides. Statistical analyses (one-way ANOVA and two-sided unpaired t-tests) were performed in R using the peptide data. The MS data have been deposited in the MassIVE repository with the dataset identifier MSV000089098.

Luciferase reporter assays

L-Wnt3A-STF cells, or HeLa, DLD-1, or SW480 cells expressing STF and Renilla-luciferase at 30LJ50% confluence were treated with the indicated compound for 16 h. The STF-firefly and Renilla luciferase activities were measured by the Dual Luciferase kit (Promega). The WNT/β-catenin pathway activities were determined by normalizing the STF-firefly activity to the Renilla activity or the total protein level. Briefly, cells were transfected with or without STF plasmid (Addgene) and pRL Renilla luciferase plasmid (Addgene) using Lipofectamine 3000 (Thermo Fisher Scientific) in Opti-MEM for 5 h and empty cloning vector as negative control. After incubating in cell growth media for 3 h, cells were collected and reseeded into 24 or 96-well plates. After incubating for 4 h, cells were treated with the indicated small molecules for 16–24 h and then washed with PBS, and then lysed with Passive Lysis Buffer (Promega) before luciferase activity was measured according to the manufacturer's instructions. Statistical analyses (one-way ANOVA and two-sided unpaired t-tests) were performed in GraphPad Prism.

BRET analysis

HAP1-TNKS1-NanoLuc cells (2×10^4 cells) treated with MG132 (1 μM) for 2 h or 293T cells (1×10^4 cells) transfected with TNKS1-NanoLuc plasmid (25 ng) for 24 h were treated with different concentrations of IWR1 in the presence of IWR1-POMA (0.5 μM) or IWR1-PEG3-NCT (0.5 μM) for 2 h in Opti-MEM without phenol red in 96-well plates. NanoBRET NanoGlo Substrate (Promega) was then added and the fluorescence signals were measured at 450 and 610 nm on a BioTek Synergy Neo2 microplate reader. The BRET signals were determined as the 610 nm (acceptor) emission over 450 nm (donor) emission ratio after background correction.

Immunofluorescence microscopy

HeLa cells at 30LJ50% confluence in a 35 mm dish were transfected with 30 ng of the indicated plasmids for 6 h and then treated with DMSO, IWR (3 μM) or IWR1-POMA (3 μM) for 16 h. Images were obtained using a Zeiss LSM 880 Airyscan confocal laser scanning microscope. FRAP analysis was performed at room temperature in the DMEM media without phenol red and with HEPES supplement and the indicated drugs. Defined regions were photobleached at a specific wavelength using the 405 nm or 561 nm laser, and the fluorescence intensities in these regions were collected every 2 s and normalized to the initial intensity before bleaching. The fluorescent signal intensities were determined in ImageJ and analyzed in GraphPad Prism.

2D colony formation assays

DLD-1, SW480, HT-29, HCT116, RKO, or DLD-1R cells were seeded into 6-well plates at 500LJ2000 cells/well with 10% FBS unless otherwise mentioned in the growth medium. Compounds were added at the indicated concentrations 16 h after seeding, and the growth medium was replenished every 3 d until colony formation was observed. The colonies were fixed with 4% formalin in PBS and stained by a solution of 0.5% crystal violet in 50% methanol solution.

3D spheroid formation assay

DLD-1 or SW480 cells were seeded at 1,000 cells/well into 96-well plates with 10% FBS in the Hyclone X growth medium. For DLD-1 cells, 3D spheroids formed 1 d after seeding. For SW480 cells, rat tail collagen I (Gibco) was added to provide the extracellular matrix, and 3D spheroids formed 5 d after seeding. Compounds were then added at the indicated concentrations. Medium with the indicated drug was replenished every 3 d, and the size of the spheroids were measured at the indicated time by imaging on a Cytation 5 Cell Imaging Multimode Reader and analyzed by Image J. The spheroids at the endpoints were fix with 4% formalin in PBS, sectioned and stained with the indicated markers after parafilm embedding.

CRC organoid formation assay

The organoids were cultured according to the procedures detailed by ATCC. Briefly, dissociated PDM-7 single cells or organoid fragments of about 200 μM diameter in size were embedded at 5,000,000 cells/mL in the cell base membrane and dispensed as small droplets onto warm 6-well plates. After solidification, the domes were covered with the advanced DMEM:F12 supplemented with HEPES, L-glutamine and B-27, noggin, gastrin, N-acetyl-cysteine, EGF, nicotinamide, A 83-01, and SB 202190 (ATCC formulation 1). The ROCK inhibitor Y-27632 (10 μM) was also included for the first 3 d of subculture. The organoids were treated with the drug 3 days after seeding for 5 days in the single-cell model and 1 day after seeding for 5 days in the organoid fragment model.

Synthetic procedures

Synthesis of IWR1-TP4-Poma (IWR1-POMA)

To a solution of [*1127442-97-0*][15] (351 mg, 0.8 mmol, 1.0 equiv) in methylene chloride (3 mL) was added methanesulfonyl chloride (183 mg, 1.6 mmol, 2.0 equiv), triethylamine (0.33 mL, 2.4 mmol, 3.0 equiv) at 0 °C. After stirring for 2 h, the reaction mixture was concentrated, the residual was re-dissolved in *N*,*N*-dimethylformamide (3 mL), and sodium azide (208 mg, 3.2 mmol, 4.0 equiv) was then added. After stirring at 50 °C overnight, the reaction was quenched with water and extracted with ethyl acetate for three times. The combined organic layers were washed with brine, dried over sodium sulfate, concentrated, and purified by silica gel flash column chromatography to give azido-IWR2 (335 mg, 90% yield) as a white powder. ^{1}H NMR (400 MHz, $CDCl_3$) δ 10.74 (s, 1H), 8.90 (dd, *J* = 6.0, 3.0 Hz, 1H), 8.78 (d, *J* = 4.4 Hz, 1H), 8.09 (d, *J* = 8.1 Hz, 2H), 7.63–7.56 (m, 2H), 7.47 (d, *J* = 4.4 Hz, 1H), 7.36 (d, *J* = 8.2 Hz, 2H), 6.28 (t, *J* = 1.8 Hz, 2H), 4.82 (s, 2H), 3.54–3.50 (m, 2H), 3.46 (dd, *J* = 3.1, 1.6 Hz, 2H), 1.79 (d, *J* = 8.6 Hz, 1H), 1.62 (d, *J* = 8.8 Hz, 1H); MS (ESI) calcd for $C_{26}H_{21}N_6O_3$ $(M+H)^+$ 465.2, found 465.2.

To a solution of azido-IWR2 (4.2 mg, 0.009 mmol, 1.0 equiv) in dimethyl sulfoxide was added [*2138439-58-2*][70] (5 mg, 0.01 mmol, 1.1 equiv), copper(II) sulfate pentahydrate (4.5 mg, 0.018 mmol, 2.0 equiv) and (+)-sodium l-ascorbate (7.2 mg, 0.036 mmol, 4.0 equiv). After stirring at 80 °C overnight, the reaction was quenched with saturated ammonium chloride and extracted with methylene chloride for three times. The combined organic layers were washed with brine, dried over sodium sulfate, concentrated, and purified by silica gel flash column chromatography followed by preparative HPLC to give IWR1-TP4-Poma (IWR1-POMA) (5.4 mg, 63% yield) as a yellow solid. ^{1}H NMR (400 MHz, $CDCl_3$) δ 10.75 (s, 1H), 8.94 (dd, *J* = 7.0, 1.9 Hz, 1H), 8.77 (d, *J* = 4.4 Hz, 1H), 8.38 (s, 1H), 8.14–8.07 (m, 2H), 7.73–7.58 (m, 3H), 7.44 (dd, *J* = 8.5, 7.1 Hz, 1H), 7.40–7.34 (m, 2H), 7.07 (dd, *J* = 7.9, 5.7 Hz, 2H), 6.85 (d, *J* = 8.5 Hz, 1H), 6.29 (t, *J* = 1.9 Hz, 2H), 6.02 (s, 2H), 4.87 (dd, *J* = 12.0, 5.4 Hz, 1H), 4.70 (s, 2H), 3.74–3.58 (m, 14H), 3.54 (dq, *J* = 3.5, 1.7 Hz, 2H), 3.49 (dd, *J* = 3.0, 1.6 Hz, 2H), 3.41 (t, *J* = 5.3 Hz, 2H), 2.89–2.66 (m, 3H), 2.14–2.04 (m, 1H), 1.82 (dt, *J* = 8.9, 1.7 Hz, 1H), 1.65 (d, *J* = 8.9 Hz, 1H); MS (ESI) calcd for $C_{50}H_{50}N_9O_{11}$ $(M+H)^+$ 952.4, found 952.3.

Synthesis of IWR1-TP(n)-Poma

Prepared using the same method as described for IWR1-TP4-Poma using pomalidomide derivatives with different PEG chain length.

IWR1-TP1-Poma:

7.4 mg, 41% yield. ^{1}H NMR (400 MHz, $CDCl_3$) δ 10.73 (s, 1H), 8.95 (dd, *J* = 6.3, 2.7 Hz, 1H), 8.74 (d, *J* = 4.3 Hz, 1H), 8.12 (dt, *J* = 9.1, 1.8 Hz, 3H), 7.71–7.61 (m, 3H), 7.44 (ddd, *J* = 8.4, 7.0, 1.1 Hz, 1H), 7.40–7.36 (m, 2H), 7.07 (d, *J* = 7.1 Hz, 1H), 7.01 (d, *J* = 4.5 Hz, 1H), 6.86 (d, *J* = 8.5 Hz, 1H), 6.29 (q, *J* = 1.6 Hz, 2H), 6.03 (s, 2H), 4.84 (dd, *J* = 12.0, 5.4 Hz, 1H), 4.71 (s, 2H), 3.74 (d, *J* = 5.3 Hz, 2H), 3.54 (dq, *J* = 3.3, 1.6 Hz, 2H), 3.50 (d, *J* = 1.1 Hz, 2H), 3.46 (d, *J* = 6.4 Hz, 2H), 2.89–2.59 (m, 3H), 1.82 (dt, *J* = 8.9, 1.5 Hz, 1H), 1.64 (d, *J* = 8.9 Hz, 1H); MS (ESI) calcd for $C_{44}H_{38}N_9O_8$ $(M+H)^+$ 820.3, found 820.2.

IWR1-TP2-Poma

10.2 mg, 76% yield. ^{1}H NMR (400 MHz, $CDCl_3$) δ 10.71 (s, 1H), 8.92 (dd, *J* = 7.4, 1.6 Hz, 1H), 8.72 (d, *J* = 4.4 Hz, 1H), 8.25 (s, 1H), 8.14–8.07 (m, 2H), 7.69–7.57 (m, 3H), 7.43–7.34 (m, 3H), 7.03 (dd, *J* = 5.9, 3.7 Hz, 2H), 6.81 (d, *J* = 8.5 Hz, 1H), 6.29 (t, *J* = 1.9 Hz, 2H), 6.01 (s, 2H), 4.87 (dd, *J* = 12.0, 5.4 Hz, 1H), 4.71 (s, 2H), 3.70 (dd, *J* = 5.9, 3.2 Hz, 2H), 3.66–3.60 (m, 4H), 3.54 (dq, *J* = 3.5, 1.7 Hz, 2H), 3.49 (d, *J* = 1.6 Hz, 4H), 3.35 (t, *J* = 5.3 Hz, 2H), 2.97–2.64 (m, 3H), 1.82 (dt, *J* = 8.9, 1.7 Hz, 1H), 1.64 (d, *J* = 8.7 Hz, 1H); MS (ESI) calcd for $C_{46}H_{42}N_9O_9$ $(M+H)^+$ 864.3, found 864.3.

IWR1-TP3-Poma

11.0 mg, 95 % yield. ^{1}H NMR (400 MHz, $CDCl_3$) δ 10.74 (s, 1H), 8.93 (dd, *J* = 6.1, 2.8 Hz, 1H), 8.78 (d, *J* = 4.4 Hz, 1H), 8.55 (s, 1H), 8.15–8.06 (m, 2H), 7.70–7.58 (m, 3H), 7.44 (dd, *J* = 8.5, 7.1 Hz, 1H), 7.40–7.35 (m, 2H), 7.09 (d, *J* = 4.4 Hz, 1H), 7.05 (d, *J* = 7.1 Hz, 1H), 6.84 (d, *J* = 8.5 Hz, 1H), 6.29 (t, *J* = 1.9 Hz, 2H), 6.01 (s, 2H), 4.93–4.85 (m, 1H), 4.70 (s, 2H), 3.76–3.59 (m, 10H), 3.54 (dq, *J* = 3.4, 1.6 Hz, 2H), 3.49 (dd, *J* = 3.0, 1.6 Hz, 2H), 3.39 (t, *J* = 5.2 Hz, 2H), 2.95–2.66 (m, 3H), 2.10 (td, *J* = 9.8, 9.0, 3.3 Hz, 1H), 1.82 (dt, *J* = 8.9, 1.7 Hz, 1H), 1.65 (d, *J* = 8.7 Hz, 1H); MS (ESI) calcd for $C_{48}H_{46}N_9O_{10}$ $(M+H)^+$ 908.3, found 908.3.

IWR1-TP5-Poma

7.6 mg, 78% yield. ^{1}H NMR (400 MHz, $CDCl_3$) δ 10.76 (s, 1H), 8.95 (dd, *J* = 7.5, 1.4 Hz, 1H), 8.77 (d, *J* = 4.4 Hz, 1H), 8.51 (s, 1H), 8.15–8.06 (m, 2H), 7.77–7.62 (m, 3H), 7.46 (dd, *J* = 8.5, 7.1 Hz, 1H), 7.42–7.33 (m, 2H), 7.21–7.14 (m, 2H), 7.10–7.03 (m, 2H), 6.87 (d, *J* = 8.5 Hz, 1H), 6.29 (t, *J* = 1.8 Hz, 2H), 6.03 (s, 2H), 4.88 (dd, *J* = 11.9, 5.4 Hz, 1H), 4.68 (s, 2H), 3.75–3.58 (m, 18H), 3.54 (dq, *J* = 3.4, 1.7 Hz, 2H), 3.48 (dd, *J* = 3.0, 1.6 Hz, 2H), 3.41 (t, *J* = 5.2 Hz, 2H), 2.91–2.63 (m, 3H), 2.10 (dt, *J* = 10.5, 4.1 Hz, 1H), 1.82 (dt, *J* = 8.9, 1.7 Hz, 1H), 1.65 (dd, *J* = 8.8, 1.6 Hz, 1H); MS (ESI) calcd for $C_{52}H_{54}N_9O_{12}$ $(M+H)^+$ 996.4, found 996.4.

IWR1-TP6-Poma

13.1 mg, 91% yield. ^{1}H NMR (400 MHz, $CDCl_3$) δ 10.75 (s, 1H), 8.94 (d, *J* = 7.5 Hz, 1H), 8.77 (d, *J* = 4.3 Hz, 1H), 8.61 (s, 1H), 8.11 (d, *J* = 8.4 Hz, 2H), 7.84–7.60 (m, 3H), 7.44 (dd, *J* = 8.5, 7.2 Hz, 1H), 7.37 (d, *J* = 8.3 Hz, 2H), 7.06 (dd, *J* = 9.4, 5.7 Hz, 2H), 6.86 (d, *J* = 8.5 Hz, 1H), 6.29 (t, *J* = 1.9 Hz, 2H), 6.04 (s, 2H),

4.88 (dd, *J* = 11.7, 5.4 Hz, 1H), 4.69 (s, 2H), 3.68 (t, *J* = 5.1 Hz, 4H), 3.64–3.56 (m, 20H), 3.55–3.51 (m, 2H), 3.48 (d, *J* = 2.1 Hz, 2H), 3.41 (t, *J* = 5.3 Hz, 2H), 2.89–2.69 (m, 3H), 2.14–2.04 (m, 1H), 1.85–1.77 (m, 1H), 1.64 (d, *J* = 8.9 Hz, 1H); MS (ESI) calcd for $C_{54}H_{58}N_9O_{13}$ $(M+H)^+$ 1040.4, found 1040.4.

Synthesis of IWR1-P(n)-Poma

To a solution of [*2472645-01-3*][71] (1.0 equiv) in methylene chloride was added amino-PEG(n)-pomalidomide (1.05 equiv) followed by 4Å molecular sieves. After stirring at 23 °C overnight, sodium triacetoxyborohydride (20 equiv) was added and the reaction was stirred for 4 h before quenched with water. The mixture was extracted with methylene chloride for three times. The combined organic layers were washed with brine, dried over sodium sulfate, concentrated, and purified by silica gel flash column chromatography followed by preparative HPLC to give IWR1-P(n)-Poma as a yellow solid.

IWR1-P1-Poma

16.0 mg, 78% yield. ^{1}H NMR (500 MHz, $CDCl_3$) δ 10.48 (s, 1H), 9.09 (s, 1H), 8.67 (t, *J* = 6.1 Hz, 2H), 7.97 (d, *J* = 8.1 Hz, 2H), 7.55 (d, *J* = 8.5 Hz, 2H), 7.43 (t, *J* = 8.0 Hz, 1H), 7.36 (t, *J* = 7.7 Hz, 1H), 7.32 (d, *J* = 8.1 Hz, 2H), 6.96 (d, *J* = 7.1 Hz, 1H), 6.76 (d, *J* = 8.6 Hz, 1H), 6.27 (t, *J* = 1.9 Hz, 2H), 4.74 (dd, *J* = 13.1, 5.3 Hz, 1H), 4.59 (s, 2H), 3.74 (s, 2H), 3.62 (t, *J* = 5.0 Hz, 2H), 3.54–3.49 (m, 2H), 3.47 (s, 4H), 3.34 (d, *J* = 5.6 Hz, 2H), 3.28–3.19 (m, 2H), 2.79–2.38 (m, 3H), 1.93 (d, *J* = 12.4 Hz, 1H), 1.80 (dt, *J* = 8.9, 1.7 Hz, 1H), 1.63 (d, *J* = 8.8 Hz, 1H); MS (ESI) calcd for $C_{43}H_{40}N_7O_8$ $(M+H)^+$ 782.3, found 782.2.

IWR1-P2-Poma

13.1 mg, 56% yield. ^{1}H NMR (500 MHz, $CDCl_3$) δ 10.53 (s, 1H), 9.39–9.14 (m, 1H), 8.71 (dd, *J* = 23.5, 5.9 Hz, 2H), 8.12–7.91 (m, 2H), 7.60 (t, *J* = 7.4 Hz, 2H), 7.49 (t, *J* = 8.2 Hz, 1H), 7.36 (d, *J* = 8.0 Hz, 2H), 7.32–7.23 (m, 2H), 7.16 (dd, *J* = 12.7, 7.1 Hz, 1H), 6.95 (d, *J* = 7.0 Hz, 1H), 6.60 (d, *J* = 8.5 Hz, 1H), 6.29 (t, *J* = 1.9 Hz, 2H), 4.91 (dd, *J* = 12.7, 5.4 Hz, 1H), 4.69 (s, 2H), 3.85 (t, *J* = 4.8 Hz, 2H), 3.68 (d, *J* = 4.3 Hz, 3H), 3.63 (dt, *J* = 10.2, 4.1 Hz, 4H), 3.58–3.45 (m, 6H), 3.39 (s, 2H), 3.22 (t, *J* = 5.1 Hz, 2H), 2.85–2.67 (m, 2H), 2.62 (td, *J* = 12.8, 4.7 Hz, 1H), 2.08–1.96 (m, 1H), 1.82 (dt, *J* = 9.0, 1.8 Hz, 1H), 1.65 (d, *J* = 8.8 Hz, 1H); MS (ESI) calcd for $C_{45}H_{44}N_7O_9$ $(M+H)^+$ 826.3, found 826.3.

IWR1-P3-Poma

13.2 mg, 72% yield. ^{1}H NMR (500 MHz, $CDCl_3$) δ 10.65 (s, 1H), 9.23 (s, 1H), 8.83 (d, *J* = 7.6 Hz, 1H), 8.75 (d, *J* = 4.0 Hz, 1H), 8.10–8.01 (m, 2H), 7.66 (t, *J* = 7.3 Hz, 2H), 7.56 (t, *J* = 8.2 Hz, 1H), 7.45–7.31 (m, 3H), 7.00 (d, *J* = 7.1 Hz, 1H), 6.74 (d, *J* = 8.6 Hz, 1H), 6.29 (d, *J* = 1.8 Hz, 2H), 4.92–4.82 (m, 1H), 4.69 (s, 2H), 3.79 (s, 2H), 3.67–3.51 (m, 14H), 3.51–3.43 (m, 4H), 3.28 (s, 2H), 2.89–2.59 (m, 3H), 2.05 (q, *J* = 9.1, 7.1 Hz, 1H), 1.85–1.77 (m, 1H), 1.64 (d, *J* = 8.9 Hz, 1H); MS (ESI) calcd for $C_{47}H_{48}N_7O_{10}$ $(M+H)^+$ 870.3, found 870.3.

IWR1-P4-Poma

15.6 mg, 68% yield. ^{1}H NMR (500 MHz, $CDCl_3$) δ 10.66 (s, 1H), 9.02 (s, 1H), 8.85 (d, *J* = 7.7 Hz, 1H), 8.76 (d, *J* = 3.9 Hz, 1H), 8.07 (d, *J* = 8.2 Hz, 2H), 7.77–7.65 (m, 2H), 7.56 (t, *J* = 8.1 Hz, 1H), 7.36 (d, *J* = 8.0 Hz, 2H), 7.32 (t, *J* = 7.8 Hz, 1H), 6.97 (d, *J* = 7.0 Hz, 1H), 6.64 (d, *J* = 8.5 Hz, 1H), 6.29 (d, *J* = 2.0 Hz, 2H), 4.87 (q, *J* = 5.7 Hz, 1H), 4.71 (s, 2H), 3.80 (s, 2H), 3.68–3.40 (m, 22H), 3.32 (s, 2H), 3.11 (d, *J* = 5.3 Hz, 2H), 2.88–2.58 (m, 3H), 2.12–2.00 (m, 1H), 1.81 (d, *J* = 8.9 Hz, 1H), 1.64 (d, *J* = 8.8 Hz, 1H); MS (ESI) calcd for $C_{49}H_{52}N_7O_{11}$ $(M+H)^+$ 914.4, found 914.3.

IWR1-P5-Poma

13.6 mg, 53% yield. ^{1}H NMR (500 MHz, $CDCl_3$) δ 10.72 (s, 1H), 8.89 (d, *J* = 7.7 Hz, 1H), 8.86 (s, 2H), 8.81 (d, *J* = 4.1 Hz, 1H), 8.10 (d, *J* = 8.0 Hz, 2H), 7.74 (dd, *J* = 13.1, 6.4 Hz, 2H), 7.60 (t, *J* = 8.1 Hz, 1H), 7.37 (dd, *J* = 8.4, 3.9 Hz, 3H), 7.24 (d, *J* = 7.6 Hz, 1H), 7.16 (dd, *J* = 12.6, 7.1 Hz, 1H), 7.01 (d, *J* = 7.1 Hz, 1H), 6.74 (d, *J* = 8.5 Hz, 1H), 6.29 (d, *J* = 1.9 Hz, 2H), 4.99–4.83 (m, 1H), 4.75 (s, 2H), 3.80 (s, 2H), 3.70–3.41 (m, 24H), 3.32 (s, 2H), 3.26 (t, *J* = 4.2 Hz, 2H), 2.76 (ddd, *J* = 61.7, 10.7, 4.5 Hz, 3H), 2.08 (dq, *J* = 7.6, 4.1, 2.7 Hz, 1H), 1.81 (d, *J* = 9.0 Hz, 1H), 1.64 (d, *J* = 8.8 Hz, 1H); MS (ESI) calcd for $C_{51}H_{56}N_7O_{12}$ $(M+H)^+$ 958.4, found 958.4.

IWR1-P6-Poma

9.2 mg, 40% yield. ^{1}H NMR (500 MHz, $CDCl_3$) δ 10.74 (s, 1H), 8.90 (d, *J* = 7.5 Hz, 2H), 8.83 (d, *J* = 4.1 Hz, 1H), 8.11 (d, *J* = 7.9 Hz, 2H), 7.76 (dd, *J* = 11.8, 6.5 Hz, 2H), 7.60 (t, *J* = 8.1 Hz, 1H), 7.38 (dd, *J* = 8.6, 2.2 Hz, 3H), 7.02 (d, *J* = 7.1 Hz, 1H), 6.73 (d, *J* = 8.5 Hz, 1H), 6.29 (t, *J* = 1.8 Hz, 2H), 4.89 (q, *J* = 5.5, 5.1 Hz, 1H), 4.77 (t, *J* = 9.9 Hz, 2H), 3.83 (s, 2H), 3.68–3.44 (m, 28H), 3.35 (s, 2H), 3.28 (d, *J* = 5.1 Hz, 2H), 2.93–2.62 (m, 3H), 2.18–2.01 (m, 1H), 1.85–1.79 (m, 1H), 1.65 (d, *J* = 8.9 Hz, 1H); MS (ESI) calcd for $C_{53}H_{60}N_7O_{13}$ $(M+H)^+$ 1002.4, found 1002.4.

Synthesis of IWR1-P(n)-VHL

Prepared as a white powder using the same method as described for IWR1-P(n)-Poma using amino-PEG(n)-VH032 derivatives[72] with different PEG chain length.

IWR1-P1-VHL

2.4 mg, 9% yield. ^{1}H NMR (400 MHz, $CDCl_3$) δ 10.75 (s, 1H), 8.97 (d, *J* = 7.7 Hz, 1H), 8.83 (d, *J* = 4.4 Hz, 1H), 8.75 (s, 1H), 8.20–8.00 (m, 2H), 7.89 (d, *J* = 4.5 Hz, 1H), 7.84 (d, *J* = 8.6 Hz, 1H), 7.71 (t, *J* = 8.1 Hz, 1H), 7.41–7.32 (m, 2H), 7.29 (s, 4H), 6.66 (d, *J* = 8.7 Hz, 1H), 6.29 (t, *J* = 1.9 Hz, 2H), 4.92 (s, 2H), 4.68–4.43 (m, 4H), 4.28 (dd, *J* = 15.2, 5.2 Hz, 1H), 4.02 (d, *J* = 11.4 Hz, 1H), 3.87 (s, 1H), 3.76 (s, 3H), 3.59 (d, *J* = 11.0 Hz, 1H), 3.55 (s, 3H), 3.49 (t, *J* = 2.3 Hz, 2H), 3.30 (q, *J* = 18.2, 15.0 Hz, 5H), 2.49 (s, 3H), 1.82 (d, *J* = 8.9 Hz, 1H), 1.65 (d, *J* = 9.0 Hz, 2H), 0.96 (s, 9H); MS (ESI) calcd for $C_{53}H_{59}N_8O_8S$ $(M+H)^+$ 967.4, found 967.4.

IWR1-P2-VHL

5.3 mg, 18% yield. ^{1}H NMR (400 MHz, $CDCl_3$) δ 10.76 (t, *J* = 2.8 Hz, 1H), 8.96 (q, *J* = 4.6, 3.7 Hz, 2H), 8.85 (q, *J* = 3.2, 2.3 Hz, 1H), 8.10 (dt, *J* = 8.7, 2.7 Hz, 2H), 7.99–7.58 (m, 5H), 7.42–7.33 (m, 4H), 7.31 (t, *J* = 2.8 Hz, 2H), 7.02 (d, *J* = 8.6 Hz, 1H), 6.47–6.13 (m, 2H), 4.90 (d, *J* = 5.4 Hz, 2H), 4.58 (td, *J* = 19.0, 16.8, 11.0 Hz, 5H), 4.31 (dd, *J* = 12.0, 8.0 Hz, 1H), 3.99 (d, *J* = 11.2 Hz, 1H), 3.85 (s, 3H), 3.70–3.60 (m, 7H), 3.55 (s, 3H), 3.50 (t, *J* = 3.2 Hz, 4H), 3.37–3.23 (m, 3H), 2.61–2.36 (m, 6H), 2.25 (d, *J* = 26.9 Hz, 3H), 1.82 (d, *J* = 9.0 Hz, 1H), 1.70–1.53 (m, 1H), 1.32 (td, *J* = 7.3, 3.4 Hz, 4H), 0.97 (d, *J* = 3.0 Hz, 10H); MS (ESI) calcd for $C_{55}H_{63}N_8O_9S$ $(M+H)^+$ 1011.4, found 1011.4.

IWR1-P3-VHL

4.7 mg, 23% yield. ^{1}H NMR (400 MHz, $CDCl_3$) δ 10.76 (s, 1H), 9.15 (s, 1H), 8.96 (d, *J* = 7.5 Hz, 1H), 8.89 (d, *J* = 4.1 Hz, 1H), 8.10 (dd, *J* = 8.6, 2.1 Hz, 2H), 7.95–7.87 (m, 1H), 7.79 (d, *J* = 8.6 Hz, 1H), 7.70 (t, *J* = 8.2 Hz, 1H), 7.38 (d, *J* = 7.9 Hz, 4H), 7.32 (d, *J* = 7.7 Hz, 2H), 6.29 (s, 2H), 4.91 (s, 2H), 4.76–4.39 (m, 4H), 3.86 (s, 2H), 3.80–3.41 (m, 17H), 3.37–3.13 (m, 2H), 2.54 (d, *J* = 2.0 Hz, 3H), 2.43 (s, 2H), 2.27 (s, 2H), 1.82 (d, *J* = 8.9 Hz, 1H), 1.65 (d, *J* = 8.8 Hz, 1H), 1.37–1.29 (m, 3H), 0.96 (s, 9H); MS (ESI) calcd for $C_{57}H_{67}N_8O_{10}S$ $(M+H)^+$ 1055.5, found 1055.4.

IWR1-P4-VHL

3.3 mg, 32% yield. ^{1}H NMR (400 MHz, $CDCl_3$) δ 10.72 (s, 1H), 8.89 (d, *J* = 7.7 Hz, 1H), 8.85–8.77 (m, 2H), 8.02 (d, *J* = 8.2 Hz, 2H), 7.81 (dd, *J* = 20.6, 6.6 Hz, 2H), 7.61 (t, *J* = 8.1 Hz, 1H), 7.36–7.23 (m, 6H), 6.91 (d, *J* = 10.9 Hz, 1H), 6.21 (t, *J* = 1.9 Hz, 2H), 4.81 (s, 2H), 4.66–4.18 (m, 5H), 3.82 (d, *J* = 20.1 Hz, 3H), 3.65–3.37 (m, 23H), 3.25 (s, 2H), 2.46 (s, 3H), 1.75 (d, *J* = 8.7 Hz, 1H), 1.57 (d, *J* = 8.9 Hz, 1H), 1.29 (t, *J* = 7.0 Hz, 3H), 0.86 (s, 9H); MS (ESI) calcd for $C_{59}H_{71}N_8O_{11}S$ $(M+H)^+$ 1099.5, found 1099.5.

IWR1-P5-VHL

6.9 mg, 32% yield. ^{1}H NMR (400 MHz, $CDCl_3$) δ 10.70 (s, 1H), 8.94 (s, 1H), 8.90 (d, *J* = 7.7 Hz, 1H), 8.82 (d, *J* = 4.0 Hz, 1H), 8.04 (d, *J* = 8.1 Hz, 2H), 7.88–7.85 (m, 1H), 7.76 (d, *J* = 8.6 Hz, 1H), 7.63 (t, *J* = 8.1 Hz, 1H), 7.30 (dd, *J* = 12.7, 7.1 Hz, 7H), 6.22 (d, *J* = 2.2 Hz, 2H), 4.85 (s, 2H), 4.72–4.35 (m, 4H), 4.27 (d, *J* = 15.0 Hz, 1H), 3.82 (s, 2H), 3.72–3.28 (m, 21H), 3.24 (d, *J* = 7.6 Hz, 3H), 2.46 (s, 3H), 1.75 (d, *J* = 8.9 Hz, 1H), 1.58 (d, *J* = 8.9 Hz, 1H), 1.28 (t, *J* = 6.8 Hz, 3H), 0.88 (s, 9H); MS (ESI) calcd for $C_{61}H_{75}N_8O_{12}S$ $(M+H)^+$ 1143.5, found 1143.4.

IWR1-P6-VHL

6.7 mg, 20% yield. ^{1}H NMR (400 MHz, $CDCl_3$) δ 10.71 (s, 1H), 9.02 (s, 1H), 8.90 (d, *J* = 7.7 Hz, 1H), 8.83 (d, *J* = 4.3 Hz, 1H), 8.10–7.99 (m, 2H), 7.86 (d, *J* = 4.4 Hz, 1H), 7.76 (d, *J* = 8.5 Hz, 1H), 7.64 (t, *J* = 8.1 Hz, 1H), 7.38–7.25 (m, 7H), 6.22 (t, *J* = 1.9 Hz, 2H), 4.87 (s, 2H), 4.50 (ddd, *J* = 35.0, 24.8, 16.4 Hz, 4H), 4.27

(dd, *J* = 15.2, 4.9 Hz, 1H), 4.02 (d, *J* = 11.3 Hz, 1H), 3.82 (d, *J* = 5.4 Hz, 2H), 3.68–3.38 (m, 32H), 3.27 (d, *J* = 7.3 Hz, 2H), 2.47 (s, 3H), 1.75 (dt, *J* = 9.0, 1.7 Hz, 1H), 1.58 (d, *J* = 8.9 Hz, 1H), 1.30 (t, *J* = 7.0 Hz, 3H), 0.89 (s, 9H); MS (ESI) calcd for $C_{63}H_{79}N_8O_{13}S$ $(M+H)^+$ 1187.5, found 1187.5.

Synthesis of IWR6-P(n)-Poma and IWR6-P(n)-VHL

Prepared using the same methods as described for IWR1-P(n)-Poma and IWR1-P(n)-VHL using [*1801530-64-2*][73].

Synthesis of IWR1-C6-Poma

Prepared using the same methods as described for IWR1-P(n)-Poma using [*2093386-50-4*][74]. MS (ESI) calcd for $C_{45}H_{44}N_7O_7$ $(M+H)^+$ 794.3, found 794.3.

Synthesis of IWR1-R-OLena

To a solution of [*2472645-01-3*][71] (40 mg, 0.09 mmol, 1.0 equiv) in methylene chloride (0.5 mL) was added [*852180-47-3*][75] (28 mg, 0.095 mmol, 1.05 equiv) followed by 4Å molecular sieves (400 mg). After stirring at 23 °C overnight, sodium triacetoxyborohydride (48 mg, 0.23 mmol, 2.5 equiv) was added and the reaction was stirred for 4 h before quenched with water. The mixture was extracted with methylene chloride for three times. The combined organic layers were washed with brine, dried over sodium sulfate, concentrated, and purified by silica gel flash column chromatography followed by preparative HPLC to give IWR1-RL (45 mg, 69% yield) as a white powder. ^{1}H NMR (400 MHz, $CDCl_3$) δ 10.82 (s, 1H), 8.89 (d, *J* = 7.8 Hz, 1H), 8.78 (dd, *J* = 4.4, 1.2 Hz, 1H), 8.16–8.03 (m, 2H), 7.67–7.62 (m, 1H), 7.61–7.53 (m, 2H), 7.41–7.34 (m, 2H), 7.27 (d, *J* = 8.0 Hz, 2H), 6.95–6.82 (m, 2H), 6.29 (q, *J* = 1.7 Hz, 2H), 4.86 (s, 4H), 4.29 (s, 2H), 3.88 (s, 2H), 3.68–3.36 (m, 8H), 3.13 (t, *J* = 5.2 Hz, 4H), 2.04 (d, *J* = 1.2 Hz, 4H), 1.81 (dd, *J* = 8.9, 1.7 Hz, 1H), 1.64 (d, *J* = 8.8 Hz, 1H), 1.48 (d, *J* = 1.3 Hz, 9H), 1.25 (td, *J* = 7.1, 1.2 Hz, 1H); MS (ESI) calcd for $C_{42}H_{45}N_6O_5$ $(M+H)^+$ 713.3, found 713.4.

To a solution of IWR1-RL (17 mg, 0.024 mmol, 1.0 equiv) in methylene chloride (0.6 mL) was added trifluoroacetic acid (0.3 L). After stirring at 40 °C overnight, the reaction mixture was concentrated and redissolved in acetonitrile (0.5 mL) before [*1323407-86-8*][76] (10.8 mg, 0.024 mmol, 1.0 equiv) and *N*,*N*-diisopropylethylamine (13 µL, 0.073 mmol, 3.0 equiv) was added. After stirring at 23 °C overnight, water was added the reaction mixture was extracted with ethyl acetate for three times. The combined organic layers were washed with brine, dried over sodium sulfate, concentrated, and purified by silica gel flash column chromatography to give IWR1-R-OLena (5.5 mg, 23% yield) as a white powder. ^{1}H NMR (400 MHz, CD_3OD) δ 9.00 (d, *J* = 4.5 Hz, 1H), 8.90 (dd, *J* = 7.3, 1.6 Hz, 1H), 8.22–8.03 (m, 2H), 7.83–7.56 (m, 8H), 7.53–7.39 (m, 7H), 7.31 (dd, *J* = 8.1, 0.9 Hz, 1H), 7.16–7.09 (m, 2H), 6.32 (t, *J* = 1.9 Hz, 2H), 5.35 (s, 2H), 5.18 (dd, *J* = 13.3, 5.2 Hz, 1H), 4.64–4.36 (m, 6H), 3.60 (dd, *J* = 3.0, 1.6 Hz, 2H), 3.48 (dq, *J* = 3.4, 1.7 Hz, 2H), 2.94 (ddd, *J* = 18.5, 13.5, 5.5 Hz, 1H), 2.81 (ddd, *J* = 17.6, 4.7, 2.4 Hz, 1H), 2.52 (qd, *J* = 13.2, 4.6 Hz, 1H), 2.21 (dtd, *J* = 12.7, 5.3, 2.5 Hz, 1H), 1.81 (dt, *J* = 8.8, 1.7 Hz, 1H), 1.73 (d, *J* = 8.8 Hz, 1H), 1.32 (s, 1H); MS (ESI) calcd for $C_{58}H_{55}N_8O_7$ $(M+H)^+$ 975.4, found 975.4.

Synthesis of G007-LK based PROTACs

Prepared using the same methods as described for the IWR1 based PROTACs.

Synthesis of IWR1-PEG3-NCT

To a solution of 6-carboxy-NCT[77] (4.0 mg, 0.0086 mmol, 1.0 equiv) in *N*,*N*-dimethylformamide (1 mL) were added *N*,*N*-diisopropylethylamine (5 µL, 0.025 mmol, 3.0 equiv) and *N*,*N*,*N*',*N*'-tetramethyl-*O*-(*N*-succinimidyl)uranium tetrafluoroborate (TSTU, 3.0 mg, 0.0010 mmol, 1.2 equiv). After stirring at 23 °C for 1 h, propargyl PEG3-amine (1.6 mg, 0.0086 mmol, 1.0 equiv) and *N*,*N*-diisopropylethylamine (2 µL, 0.017 mmol, 2.0 equiv) in *N*,*N*-dimethylformamide (0.5 mL) were added. The reaction mixture was stirred at 23 °C for 45 min before concentrated and purified by preparative HPLC to give 6-(propargyl-PEG3-carbamoyl)-NCT (3.5 mg, 56% yield). MS (ESI) calcd for $C_{44}H_{50}N_3O_7$ $(M+H)^+$ 732.4, found 732.3.

To a solution of azido-IWR2 (1.2 mg, 0.0027 mmol, 1.0 equiv) in aqueous acetonitrile (67%, 2.25 mL) was added 6-(propargyl-PEG3-carbamoyl)-NCT (2.0 mg, 0.0027 mmol, 1.1 equiv), copper powder (1.0 mg, 0.0013 mmol, 0.5 equiv). After stirring at 23 °C for 16 h, the reaction mixture was filtered, concentrated, and purified by preparative HPLC to give IWR1-PEG3-NCT (1.0 mg, 31% yield) as a blue solid. ^{1}H NMR (600 MHz, MeOD) δ 8.75 (dd, *J* = 15.4, 5.9 Hz, 2H), 8.28 (d, *J* = 8.2 Hz, 1H), 8.11–8.08 (m, 1H), 8.05 (d, *J* = 8.8 Hz, 2H), 7.85 (d, *J* = 8.5 Hz, 1H), 7.78 (s, 1H), 7.57 (t, *J* = 8.1 Hz, 1H), 7.42 (d, *J* = 8.2 Hz, 1H), 7.38 (d, *J* = 8.1 Hz, 1H), 7.07 (d, *J* = 4.4 Hz, 1H), 6.53 (s, 1H), 6.34–6.22 (m, 2H), 6.14 (s, 1H), 5.95 (s, 1H), 5.35 (t, *J* = 5.0 Hz, 1H), 4.58 (s, 2H), 3.86 (q, *J* = 9.2 Hz, 2H), 3.70–3.63 (m, 4H), 3.61 (s, 2H), 3.60–3.56 (m, 4H), 3.49 (t, *J* = 5.8 Hz, 2H), 3.47–3.40 (m, 4H), 3.19 (m, 1H), 2.97–2.85 (m, 4H), 2.75–2.64 (m, 2H), 2.61 (d, *J* = 7.9 Hz, 2H), 2.52–2.43 (m, 4H), 2.28 (t, *J* = 7.4 Hz, 2H), 2.23– 2.15 (m, 2H), 2.13 (s, 1H), 2.02 (d, *J* = 13.6 Hz, 4H), 1.91–1.84 (m, 2H), 1.70 (s, 4H), 1.60 (d, *J* = 5.9 Hz, 4H); MS (ESI) calcd for $C_{70}H_{69}N_9O_{10}$ $(M+H)^+$ 1195.5, found 1196.3.

Supplementary figures

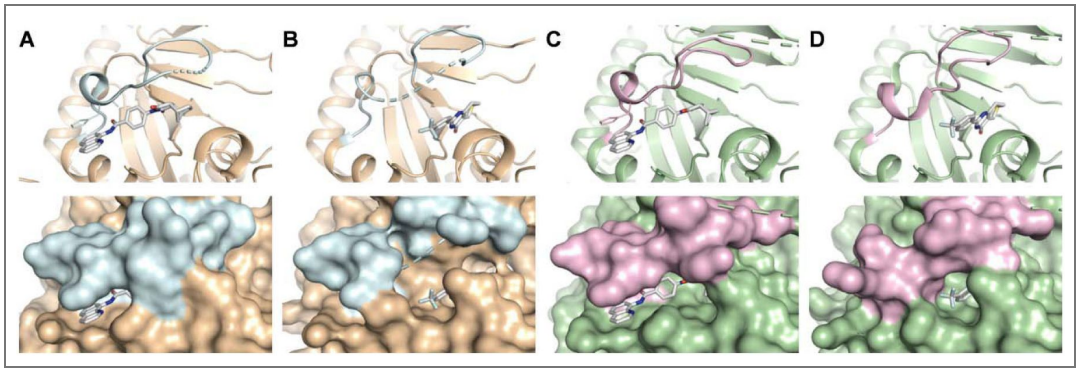

Figure S1. Crystal structures used to guide the design of PROTAC molecules (A) The crystal structure of TNKS1 with IWR1-exo (PDB 4OA7). (B) The crystal structure of TNKS1 with XAV939 (PDB 3UH4). (C) The crystal structure of TNKS2 with IWR1 (PDB 3UA9). (D) The crystal structure of TNKS2 with XAV939 (PDB 3KR8).

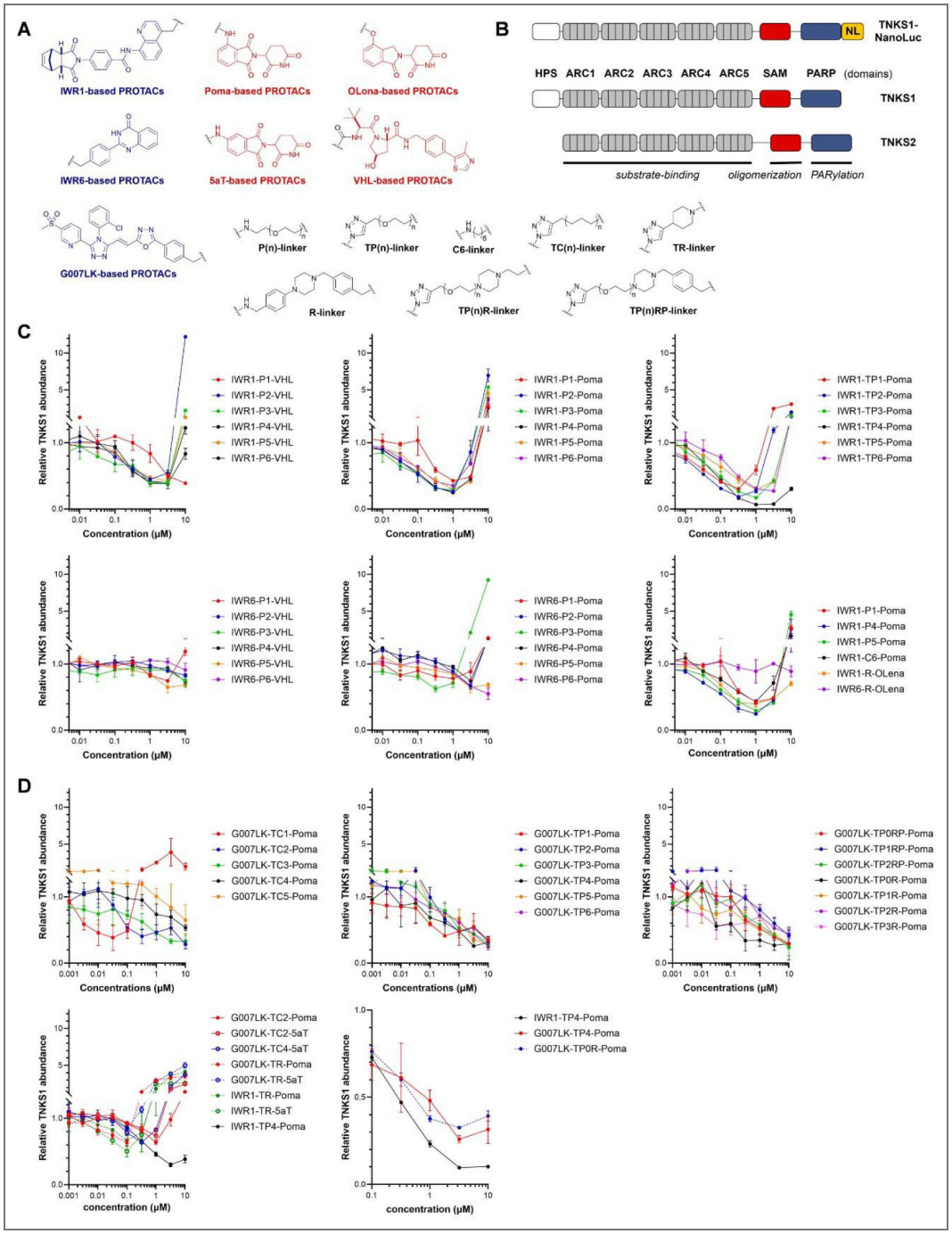

Figure S2. Identification of active PROTAC molecules using CRISPR engineered HAP1 cells expressing a TNKS1- NanoLuc fusion protein

(A) Chemical structures of the PROTAC molecules. (B) Schematic diagrams of the domain structures of TNKS1, TNKS2 and TNKS1-NanoLuc. (C) Relative abundance of the endogenous TNKS1 measured by the luciferase activity upon treating HAP1-TNKS1-NanoLuc cells with IWR1-P(n)-VHL, IWR6-P(n)-VHL, IWR1-P(n)-Poma, IWR6-P(n)-Poma, or IWR1-TP(n)-Poma. IWR1-R-Olena bearing a rigid linker of length and polarity comparable to IWR1-P4-Poma and IWR1-P5-Poma alleviated the hook effect but was less effectively in promoting TNKS1 degradation. Removing the oxygen atom from the linker of IWR1-P1-Poma gave IWR1-C6-Poma with a more hydrophobic linker, but there was no improvement in the degradation efficacy. At high PROTAC concentrations, binding of TNKS and CRBN/VHL by separate PROTAC molecules impedes the formation of productive ternary complexes, resulting in reduced degradation efficacy and consequently the hook effect. Under these conditions, PROTAC molecules function as catalytic inhibitors to prevent TNKS turnover, leading to TNKS accumulation. Data are presented as mean ± SEM (n = 3 biological samples). (D) Selected SAR of PROTACs using G007-LK as the warhead. When shown, IWR1-POMA was included in the assay for direction comparison. All data are presented as mean ± SEM (n = 3 biological samples).

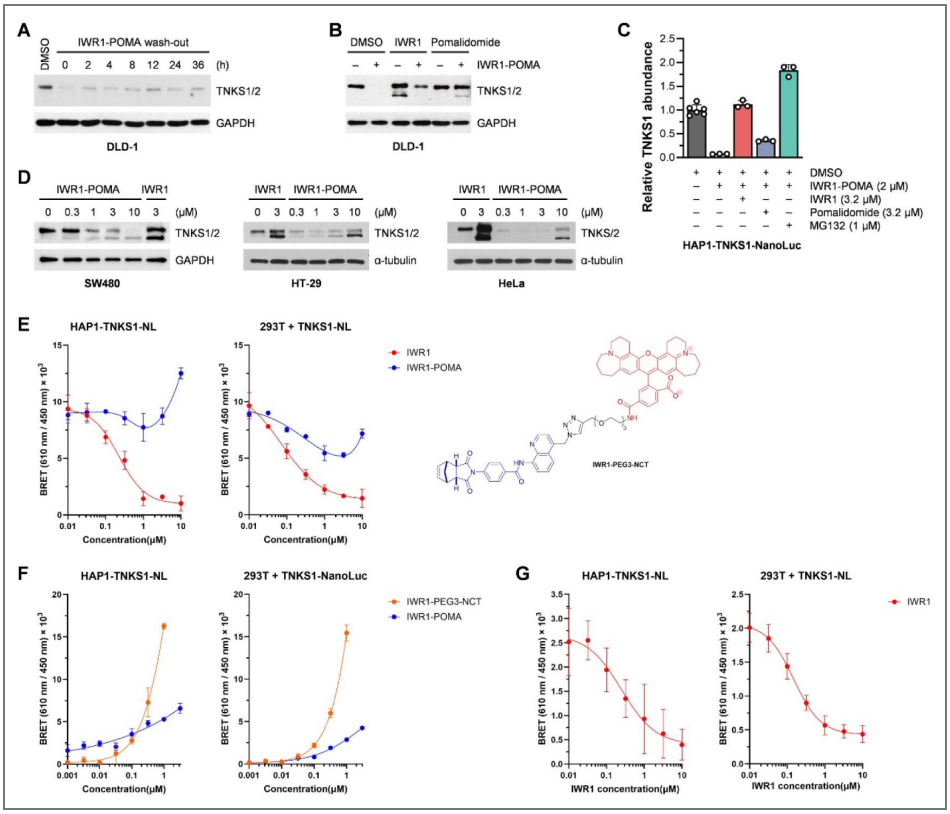

Figure S3. Additional characterization of IWR1-POMA

(A) TNKS did not recover in DLD-1 cells at least 36 h after removing IWR1-POMA. (B) IWR1 (3 μM) and pomalidomide (3 μM) prevented the degradation of TNKS by IWR1-POMA (3 μM) in DLD-1 cells. (C) IWR1, pomalidomide, and MG132 blocked the degradation of TNKS by IWR1-POMA in HAP1-TNKS-NanoLuc cells. (D) IWR1-POMA promoted TNKS degradation while IWR1 induced TNKS accumulation in SW480, HT-29 and HeLa cells. (E) IWR1 suppressed the BRET signals of IWR1-PEG3-NCT (0.5 μM) with an IC_{50} value of 0.23 μM in HAP1-TNKS1-NanoLuc cells pretreated with MG132 for 16 h or with an IC_{50} value of 0.07 μM in 293T cells transfected with TNKS1-NanoLuc plasmid (25 ng). However, the intrinsic fluorescence of IWR1-POMA prevented the determination of its binding to TNKS1 by this method. Data are presented as mean ± SEM (n = 3 biological samples). (F) Addition of IWR1-PEG3-NCT or IWR1-POMA increased BRET signals in a dose-dependent manner in HAP1-TNKS1-NanoLuc cells pretreated with MG132 for 16 h or in 293T cells transfected with TNKS1-NanoLuc plasmid (25 ng). Data are presented as mean ± SEM (n = 3 biological samples). (G) IWR1 suppressed the BRET signals of IWR1-POMA (0.5 μM) with an IC_{50} value of 0.25 μM in HAP1-TNKS1-NanoLuc cells pretreated with MG132 for 16 h or with an IC_{50} value of 0.15 μM in 293T cells transfected with TNKS1-NanoLuc plasmid (25 ng). Data are presented as mean ± SEM (n = 6 biological samples).

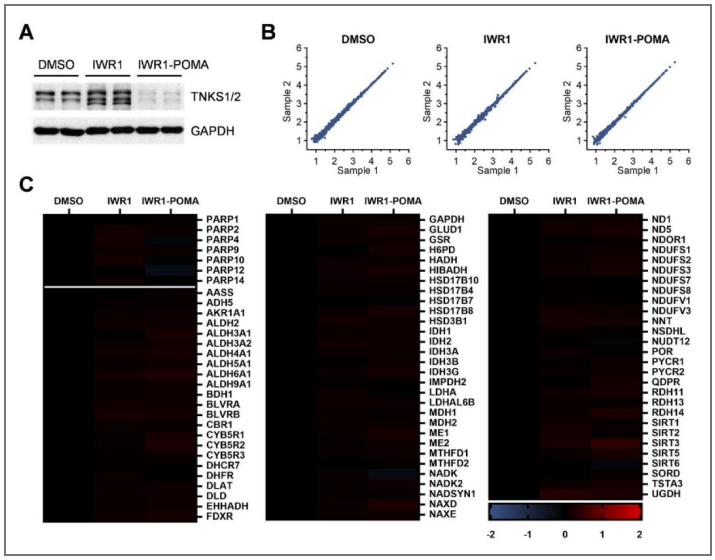

Figure S4. Proteomic analysis of DLD-1 cells treated with DMSO, IWR1 or IWR1-POMA

(A) Western blot analysis of samples corresponding to Figure 1 E and 1F confirmed the accumulation of TNKS1/2 by IWR1 and the depletion by IWR1-POMA. (B) Correlation analysis showed high reproducibility between the two biological samples. (C) IWR1-POMA selectively degraded TNKS without inducing appreciable perturbations to 7 other PARP family member proteins and 79 NAD(P)-dependent enzymes detected in this proteomic experiment.

Figure S5. Degradation of TNKS by IWR1-POMA in 293T cells

(A) 293T cells were transfected with different doses of Wnt3A plasmid and then treated with DMSO, IWR1 (3 μM) or IWR1-POMA (3 μM). The cytosolic fraction of the cell lysates was then examined by Western blot. IWR1-POMA promoted a more complete degradation of β-catenin than IWR1 and reduced the level of the WNT target AXIN2. (B) Western blot analysis confirmed the lack of TNKS expression in 293T-TNKS1/2-DKO cells and validated the expression of FLAG-TNKS1, 3×FLAG-TNKS1-PD, FLAG-TNKS2 and FLAG-TNKS2-M1054V after transfection. (C) Western blot analysis of samples corresponding to Figure 2A confirmed the degradation of TNKS1 by IWR1-POMA. (D) Western blot analysis of samples corresponding to Figure 2B confirmed the degradation of TNKS2 by IWR1-POMA. (E) Western blot analysis of samples corresponding to Figure 2C confirmed the degradation of TNKS1-PD by IWR1-POMA. (F) Western blot analysis of samples corresponding to Figure 2D confirmed the degradation of TNKS2-M1054V by IWR1-POMA. (G) Comparison of the effects of IWR1 and IWR1-POMA on WNT/β-catenin pathway activity in 293T-TNKS1/2-DKO cells, related to Figure 2. Data were normalized to the STF activity of the IWR1-treated samples at the indicated concentrations to combine results from three independent experiments for statistical analysis. Data are presented as mean ± SEM (n = 3×3 biological samples) with p-values calculated by two-tailed unpaired t-test.

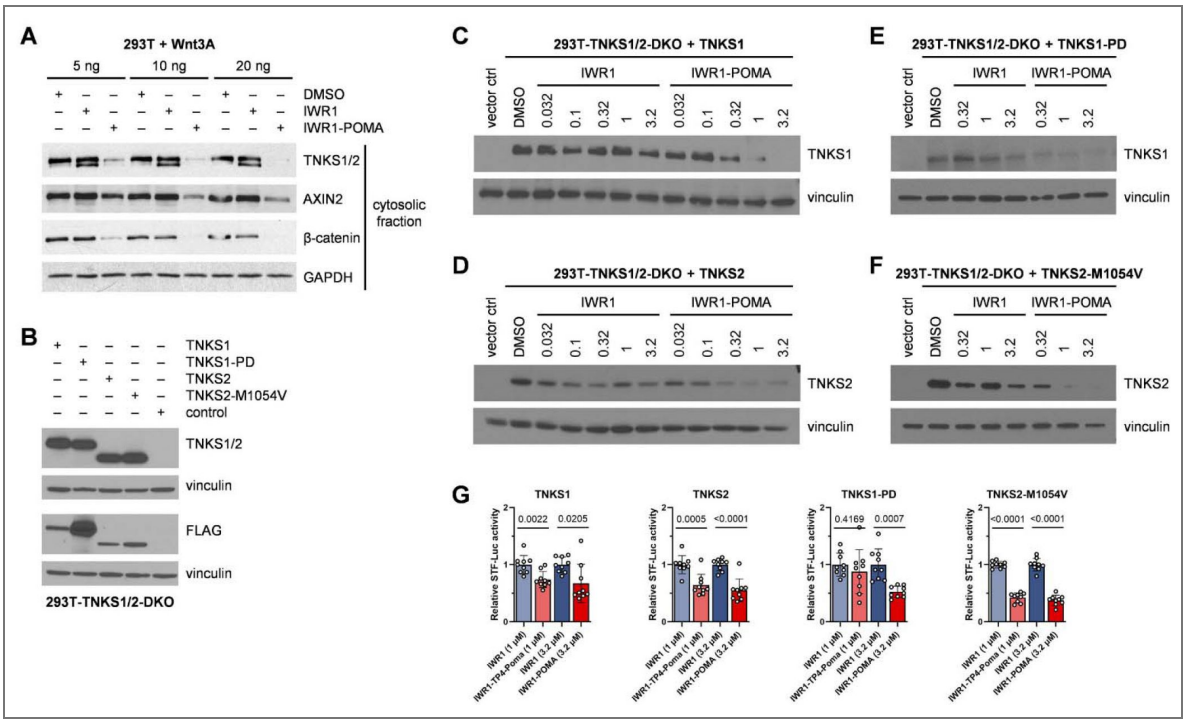

Figure S6. Effects of TNKS on AXIN puncta

Additional images of 293T or 293T-TNKS1/2-DKO cells transfected with or without TNKS plasmids from independent experiments related to Figure 3.

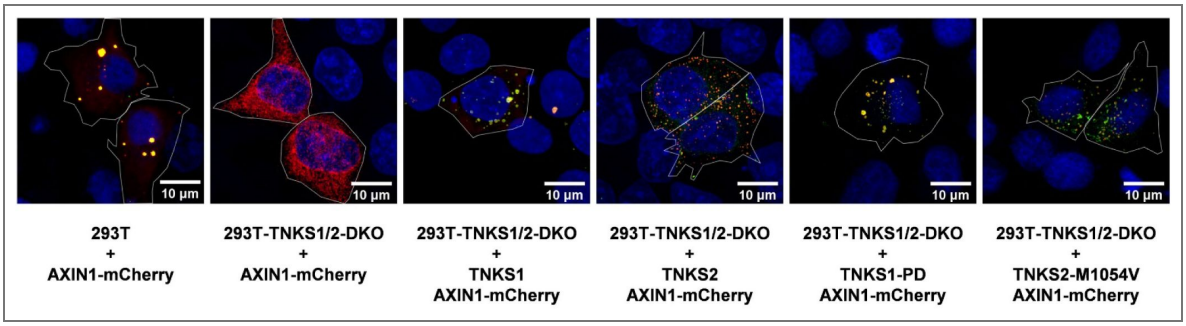

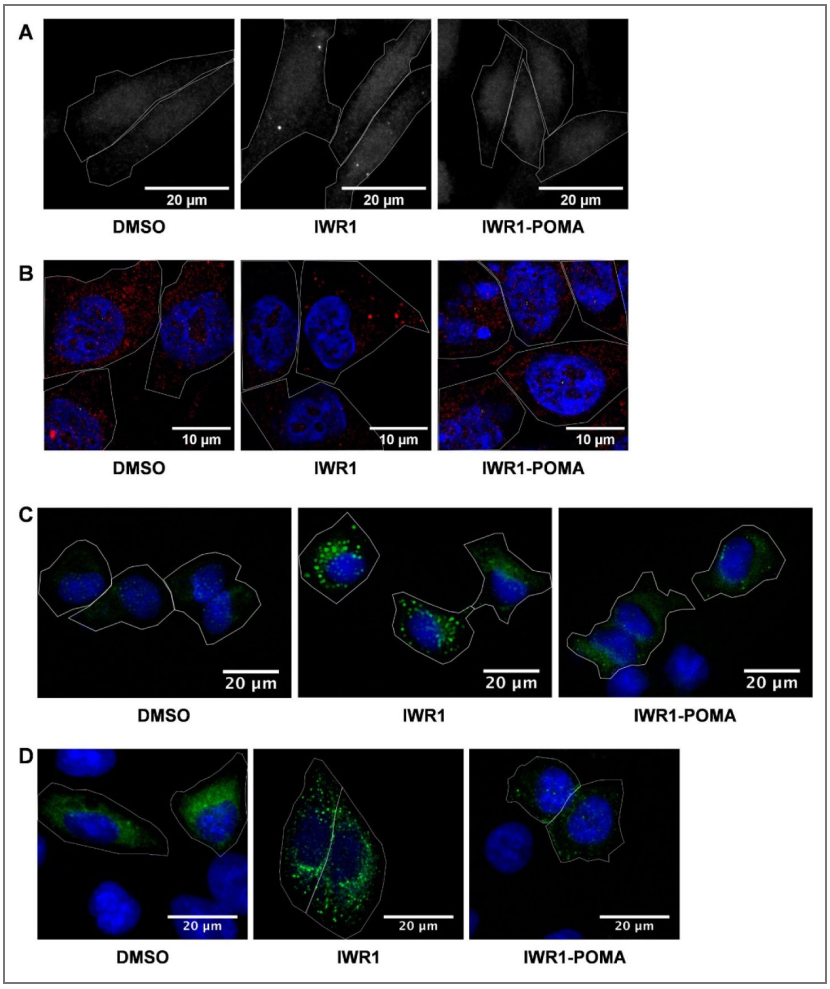

Figure S7. TNKSi induced the formation of AXIN puncta

(A) Additional images of SW480 cells treated with DMSO, IWR1 (5 μM), or IWR1-POMA (1 μM), related to Figure 4A. (B) Multi-channel images of HEK293-AXIN1-dsRed-KI cells treated with DMSO, IWR1 (3 μM), or IWR1-POMA (3 μM) with nuclear staining (DAPI, blue), corresponding to Figure 4C. (C) HeLa cells transfected with GFP-AXIN1 plasmid followed by treating with DMSO, IWR1 (3 μM), or IWR1-POMA (3 μM). Together with Figure 4C, this experiment shows that the position of GFP tag does not affect puncta formation. (D) HeLa cells transfected with GFP-AXIN2 plasmid followed by treating with DMSO, IWR1 (3 μM), or IWR1-POMA (3 μM). This experiment shows that AXIN2 also forms puncta upon IWR1 treatment.

Figure S8. IWR1-POMA suppressed CRC growth through WNT inhibition

(A) IWR1-POMA suppressed the formation of DLD-1 colonies more effectively than IWR1 under both normal and low serum conditions. Data are presented as mean ± SEM (n = 3–4 biological samples) with p-values calculated by two-tailed unpaired t-test. (B) Quantification of SW480 and HT-29 colonies, related to Figure 6A. Data are presented as mean ± SEM (n = 3–5 biological samples) with p-values calculated by two-tailed unpaired t-test. (C) IWR1-POMA (3 μM) suppressed of WNT signaling more effectively than IWR1 (3 μM) in DLD-1 and SW480 cells. Data are presented as mean ± SEM (n = 3 biological samples) with p-values calculated by two-tailed unpaired t-test. (D) Western blot analysis confirmed that c-MYC, Aurora A, CDK4 and cyclin D1 responded to IWR1-POMA (3 μM) but not IWR1 (3 μM) in DLD-1 cells.

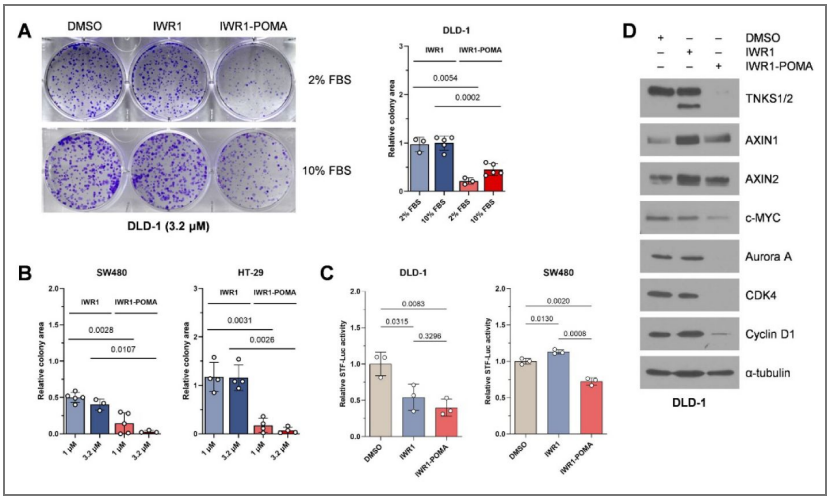

Figure S9. IWR1-POMA suppressed CRC proliferation through on-target WNT inhibition

(A) Quantification of HCT116 colonies, related to Figure 6B. Data are presented as mean ± SEM (n = 3–4 biological samples). (B) IWR1-POMA (3 μM) reduced the cytosolic β-catenin level more effectively than IWR1 (3 μM) in 293T cells. The level of cytosolic β-catenin in 293T-TNKS1/2-DKO cells that lack both TNKS1 and TNKS2 did not change significantly with either drug treatment. (C) CC-90009 induced GSPT1 degradation in DLD-1 cells but had little effect on TNKS. GSPT2 was not detectable by Western blot, which is consistent with the reported GSPT levels determined by quantitative proteomic analysis in this cell line —102,567 ppb for GSPT1 and 2,495 ppb for GSPT2 (*https://www.ebi.ac.uk/gxa/experiments/E-PROT-18/Results*)[68]. (D) DLD-1R cells obtained from cultivating DLD-1 cells with CC-90009 have a dramatically reduced level of GSPT1 expression meanwhile maintaining normal TNKS expression. (E) IWR1 (3 μM) promoted TNKS accumulation while IWR1-POMA (3 μM) induced TNKS degradation in DLD-1R cells. (F) IWR1-POMA prevented colony formation of DLD-1R cells deficient in GSPT1/2. Data are presented as mean ± SEM (n = 3 biological samples) with p-values calculated by two-tailed unpaired t-test. (G) Quantification of RKO colonies, related to Figure 6B. Data are presented as mean ± SEM (n = 3 biological samples) with p-values calculated by two-tailed unpaired t-test.

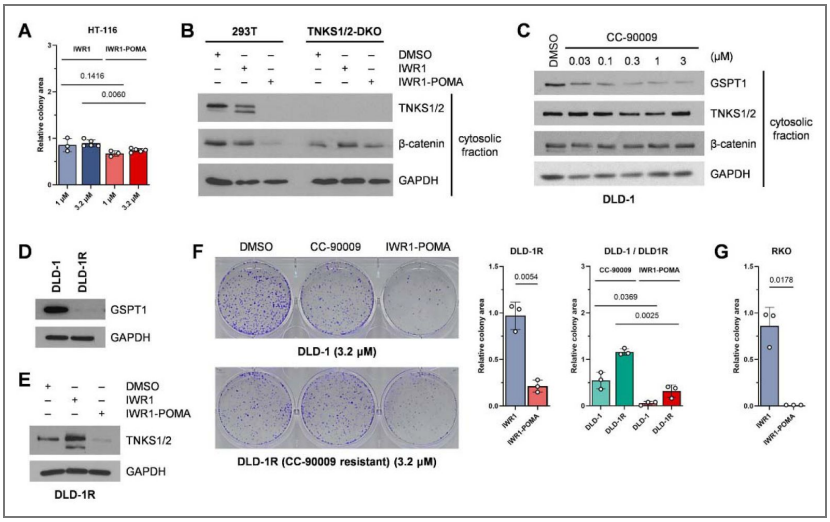

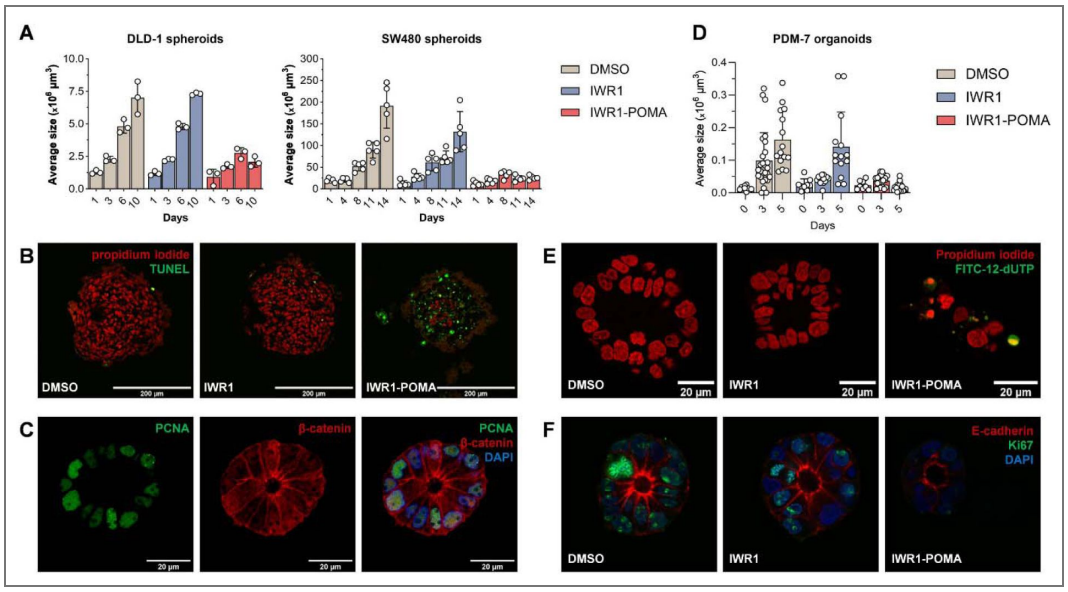

Figure S10. IWR1-POMA demonstrated efficacy in CRC spheroid and primary organoid models

(A) The growth chart of DLD-1 and SW480 spheroids treated with DMSO, IWR1 (5 μM), or IWR1-POMA (5 μM). The sizes represent the apparent dimensions of the spheroids including the peripheral dead cells. Data are presented as mean ± SEM (n = 3 or 5 biological samples) with p-values calculated by two-tailed unpaired t-test. (B) IWR1-POMA (5 μM) induced apoptosis in DLD-1 spheroids. (C) PDM-7 organoids grown from single cells preserved the heterogeneous nature of CRC tumors. (D) IWR1-POMA (1 μM) suppressed the formation of PDM-7 organoids from single cells while IWR1 (1 μM) did not. Data are presented as mean ± SEM (n = 8–27 biological samples) with p-values calculated by two-tailed unpaired t-test. (E and F) IWR1-POMA (1 μM) suppressed proliferation and induced apoptosis in PDM-7 organoids grown from single cells while IWR1 (1 μM) had little effect.

Data availability

The MS data have been deposited in the MassIVE repository with the dataset identifier MSV000089098.

Acknowledgements

We thank Dr. Susan Smith (New York University) for providing 293T-TNKS1/2-DKO cells and FLAG-TNKS1-PD construct, Dr. Mariann Bienz and Dr. Melissa Gammons (MRC Laboratory of Molecular Biology) for 293T-DVL2-GFP/AXIN1-dsRed cells and AXIN1-GFP construct, Dr. Dominic Bernkopf (Friedrich-Alexander University Erlangen-Nürnberg) for GFP-AXIN1 and GFP-AXIN2 constructs. We also thank Dr. Katherine Phelps and Dr. Marcel Mettlen for assistance in immunofluorescence microscopy experiments, Dr. Min Fang in automated liquid dispensing and handling, John Shelton in spheroid sectioning, Qing Ding in TMT labeling, and Dr. Duojia Pan, Dr. Xuewu Zhang, Dr. Michael Cohen (Oregon Health & Science University), and Dr. Mike White (IDEAYA Bioscience) for helpful discussions. This work is supported by National Institutes of Health grant R01 CA269377 (to C.C.), R35 GM134883 (to Y.Y.), and P30 CA142543 (to J.W.S.).

Additional files

supplementary information

Additional information

Funding

Funder	Grant reference number	Author
HHS | National Institutes of Health (NIH)	R01 CA269377	Chuo Chen
HHS | National Institutes of Health (NIH)	R35 GM134883	Yonghao Yu
HHS | National Institutes of Health (NIH)	P30 CA142543	Jerry W Shay

Author ORCID iDs

Andrew Lemoff: https://orcid.org/0000-0002-4943-0170
Lawrence Lum: https://orcid.org/0000-0002-6119-0253
Chuo Chen: https://orcid.org/0000-0002-3118-4901

References

1. **Nusse R,** Clevers H (2017) Wnt/β-Catenin Signaling, Disease, and Emerging Therapeutic Modalities. *Cell* **169**:985-999 https://doi.org/10.1016/j.cell.2017.05.016 | PubMed
2. **Clevers H,** Nusse R (2012) Wnt/β-Catenin Signaling and Disease. *Cell* **149**:1192-1205 https://doi.org/10.1016/j.cell.2012.05.012 | PubMed
3. **Zhang L,** Shay JW (2017) Multiple Roles of APC and its Therapeutic Implications in Colorectal Cancer. *J. Natl. Cancer Inst* **109**:djw332 https://doi.org/10.1093/jnci/djw332 | PubMed
4. **Zhong Z,** Virshup DM (2020) Wnt Signaling and Drug Resistance in Cancer. *Mol. Pharmacol* **97**:72-89 https://doi.org/10.1124/mol.119.117978 | PubMed
5. **Hsiao SJ,** Smith S (2008) Tankyrase Function at Telomeres, Spindle Poles, and Beyond. *Biochimie* **90**:83-92 https://doi.org/10.1016/j.biochi.2007.07.012 | PubMed
6. **Haikarainen T,** Krauss S, Lehtiö L (2014) Tankyrases: Structure, Function and Therapeutic Implications in Cancer. *Curr. Pharm. Des* **20**:6472-6488 https://doi.org/10.2174/13816128206614063010152 5 | PubMed

7. **Mariotti L,** Pollock K, Guettler S (2017) Regulation of Wnt/β-catenin Signalling by Tankyrase-dependent Poly(ADP-ribosyl)ation and Scaffolding. *Br. J. Pharmacol* **174**:4611-4636 https://doi.org/10.1111/bph.14038 | PubMed
8. **Schatoff EM,** Goswami S, Zafra MP, Foronda M, Shusterman M, Leach BI, Katti A, Diaz BJ, Dow LE (2019) Distinct Colorectal Cancer–Associated APC Mutations Dictate Response to Tankyrase Inhibition. *Cancer Discov* **9**:1358-1371 https://doi.org/10.1158/2159-8290.cd-19-0289 | PubMed
9. **Schaefer KN,** Peifer M (2019) Wnt/Beta-Catenin Signaling Regulation and a Role for Biomolecular Condensates. *Dev. Cell* **48**:429-444 https://doi.org/10.1016/j.devcel.2019.01.025 | PubMed
10. **Bienz M** (2020) Head-to-Tail Polymerization in the Assembly of Biomolecular Condensates. *Cell* **182**:799-811 https://doi.org/10.1016/j.cell.2020.07.037 | PubMed
11. **Gammons M,** Bienz M (2018) Multiprotein Complexes Governing Wnt Signal Transduction. *Curr. Opin. Cell Biol* **51**:42-49 https://doi.org/10.1016/j.ceb.2017.10.008 | PubMed
12. **Huang S.-MA,** Mishina YM, Liu S, Cheung A, Stegmeier F, Michaud GA, Charlat O, Wiellette E, Zhang Y, Wiessner S, *et al.* (2009) Tankyrase Inhibition Stabilizes Axin and Antagonizes Wnt Signalling. *Nature* **461**:J620 https://doi.org/10.1038/nature08356 | PubMed
13. **Zhang Y,** Liu S, Mickanin C, Feng Y, Charlat O, Michaud GA, Schirle M, Shi X, Hild M, Bauer A, *et al.* (2011) RNF146 is a Poly(ADP-ribose)-directed E3 Ligase that Regulates Axin Degradation and Wnt Signalling. *Nat. Cell Biol* **13**:623-629 https://doi.org/10.1038/ncb2222 | PubMed
14. **DaRosa PA,** Wang Z, Jiang X, Pruneda JN, Cong F, Klevit RE, Xu W (2015) Allosteric Activation of the RNF146 Ubiquitin Ligase by a Poly(ADP-ribosyl)ation Signal. *Nature* **517**:223-226 https://doi.org/10.1038/nature13826 | PubMed
15. **Chen B,** Dodge ME, Tang W, Lu J, Ma Z, Fan C.-W, Wei S, Hao W, Kilgore J, Williams NS, *et al.* (2009) Small Molecule–Mediated Disruption of Wnt-dependent Signaling in Tissue Regeneration and Cancer. *Nat. Chem. Biol* **5**:100-107 https://doi.org/10.1038/nchembio.137 | PubMed
16. **de la Roche M,** Ibrahim AEK, Mieszczanek J, Bienz M (2014) LEF1 and B9L Shield β-Catenin from Inactivation by Axin, Desensitizing Colorectal Cancer Cells to Tankyrase Inhibitors. *Cancer Res* **74**:1495-1505 https://doi.org/10.1158/0008-5472.can-13-2682 | PubMed
17. **Thorvaldsen TE,** Pedersen NM, Wenzel EM, Schultz SW, Brech A, Liestøl K, Waaler J, Krauss S, Stenmark H (2015) Structure, Dynamics, and Functionality of Tankyrase Inhibitor-Induced Degradasomes. *Mol. Cancer Res* **13**:1487-1501 https://doi.org/10.1158/1541-7786.mcr-15-0125 | PubMed
18. **Martino-Echarri E,** Brocardo MG, Mills KM, Henderson BR (2016) Tankyrase Inhibitors Stimulate the Ability of Tankyrases to Bind Axin and Drive Assembly of β-Catenin Degradation-Competent Axin Puncta. *PLoS One* **11**:e0150484 https://doi.org/10.1371/journal.pone.0150484 | PubMed
19. **Mariotti L,** Templeton CM, Ranes M, Paracuellos P, Cronin N, Beuron F, Morris E, Guettler S (2016) Tankyrase Requires SAM Domain-Dependent Polymerization to Support Wnt-β-Catenin Signaling. *Mol. Cell* **63**:498-513 https://doi.org/10.1016/j.molcel.2016.06.019 | PubMed
20. **Schreiber SL** (2021) The Rise of Molecular Glues. *Cell* **184**:3-9 https://doi.org/10.1016/j.cell.2020.12.020 | PubMed
21. **Chirnomas D,** Hornberger KR, Crews CM (2023) Protein Degraders Enter the Clinic — A New Approach to Cancer Therapy. *Nat. Rev. Clin. Oncol* **20**:265-278 https://doi.org/10.1038/s41571-023-00736-3 | PubMed
22. **Shin Y,** Brangwynne CP (2017) Liquid Phase Condensation in cell Physiology and Disease. *Science* **357**:eaaf4382 https://doi.org/10.1126/science.aaf4382 | PubMed
23. **Banani SF,** Lee HO, Hyman AA, Rosen MK (2017) Biomolecular Condensates: Organizers of Cellular Biochemistry. *Nat. Rev. Mol. Cell Biol* **18**:285-298 https://doi.org/10.1038/nrm.2017.7 | PubMed
24. **Kulak O,** Chen H, Holohan B, Wu X, He H, Borek D, Otwinowski Z, Yamaguchi K, Garofalo LA, Ma Z, *et al.* (2015) Disruption of Wnt/β-catenin Signaling and Telomeric Shortening Are Inextricable Consequences of Tankyrase Inhibition in Human Cells. *Mol. Cell Biol* **35**:2425-2435 https://doi.org/10.1128/mcb.00392-15 | PubMed

25. **Winter GE,** Buckley DL, Paulk J, Roberts JM, Souza A, Dhe-Paganon S, Bradner JE (2015) Phthalimide Conjugation as a Strategy for In Vivo Target Protein Degradation. *Science* **348**:1376-1381 https://doi.org/10.1126/science.aab1433 | PubMed

26. **Galdeano C,** Gadd MS, Soares P, Scaffidi S, Van Molle I, Birced I, Hewitt S, Dias DM, Ciulli A (2014) Structure-Guided Design and Optimization of Small Molecules Targeting the Protein–Protein Interaction between the von Hippel–Lindau (VHL) E3 Ubiquitin Ligase and the Hypoxia Inducible Factor (HIF) Alpha Subunit with in Vitro Nanomolar Affinities. *J. Med. Chem* **57**:8657-8663 https://doi.org/10.1021/jm5011258 | PubMed

27. **Schmid-Burgk JL,** Höning K, Ebert TS, Hornung V (2016) CRISPaint Allows Modular Base-specific Gene Tagging Using A Ligase-4-dependent Mechanism. *Nat. Commun* **12338** https://doi.org/10.1038/ncomms12338 | PubMed

28. **Lau T,** Chan E, Callow M, Waaler J, Boggs J, Blake RA, Magnuson S, Sambrone A, Schutten M, Firestein R, *et al.* (2013) A Novel Tankyrase Small-Molecule Inhibitor Suppresses APC Mutation–Driven Colorectal Tumor Growth. *Cancer Res* **73**:3132-3144 https://doi.org/10.1158/0008-5472.can-12-4562 | PubMed

29. **Robers MB,** Dart ML, Woodroofe CC, Zimprich CA, Kirkland TA, Machleidt T, Kupcho KR, Levin S, Hartnett JR, Zimmerman K, *et al.* (2015) Target Engagement and Drug Residence Time Can Be Observed in Living Cells with BRET. *Nat. Commun* **6**:10091 https://doi.org/10.1038/ncomms10091 | PubMed

30. **Kampmann SS,** Skelton BW, Yeoh GC, Abraham LJ, Lengkeek NA, Stubbs KA, Heath CH, Stewart SG (2015) The Synthesis and Fluorescence Profile of Novel Thalidomide Analogues. *Tetrahedron* **71**:8140-8149 https://doi.org/10.1016/j.tet.2015.08.036

31. **Weihs F,** Wang J, Pfleger KDG, Dacres H (2020) Experimental Determination of the Bioluminescence Resonance Energy Transfer (BRET) Förster Distances of NanoBRET and Red-shifted BRET Pairs. *Anal Chim Acta X* **6**:100059 https://doi.org/10.1016/j.acax.2020.100059 | PubMed

32. **Bhardwaj A,** Yang Y, Ueberheide B, Smith S (2017) Whole Proteome Analysis of Human Tankyrase Knockout Cells Reveals Targets of Tankyrase-mediated Degradation. *Nat. Commun* **8**:2214 https://doi.org/10.1038/s41467-017-02363-w | PubMed

33. **Cook BD,** Chang JNDW, Shostak G, Smith S (2002) Role for the Related Poly(ADP-Ribose) Polymerases Tankyrase 1 and 2 at Human Telomeres. *Mol. Cell Biol* **22**:332-342 https://doi.org/10.1128/mcb.22.1.332-342.2002 | PubMed

34. **Sbodio JI,** Lodish HF, Chi N.-W (2002) Tankyrase-2 Oligomerizes with Tankyrase-1 and Binds to Both TRF1 (Telomere-repeat-binding Factor 1) and IRAP (Insulin-responsive Aminopeptidase). *Biochem. J* **361**:451-459 https://doi.org/10.1042/0264-6021:3610451 | PubMed

35. **Riccio AA,** McCauley M, Langelier M.-F, Pascal JM (2016) Tankyrase Sterile α Motif Domain Polymerization Is Required for Its Role in Wnt Signaling. *Structure* **24**:1573-1581 https://doi.org/10.1016/j.str.2016.06.022 | PubMed

36. **Kan W,** Enos MD, Korkmazhan E, Muennich S, Chen D.-H, Gammons MV, Vasishtha M, Bienz M, Dunn AR, Skiniotis G, *et al.* (2020) Limited Dishevelled/Axin Oligomerization Determines Efficiency of Wnt/b-catenin Signal Transduction. *eLife* **9**:e55015 https://doi.org/10.7554/eLife.55015 | PubMed

37. **Behrens J,** Jerchow B.-A, Würtele M, Grimm J, Asbrand C, Wirtz R, Kühl M, Wedlich D, Birchmeier W (1998) Functional Interaction of an Axin Homolog, Conductin, with β-Catenin, APC, and GSK3β. *Science* **280**:596-599 https://doi.org/10.1126/science.280.5363.596 | PubMed

38. **Spink KE,** Polakis P, Weis WI (2000) Structural Basis of the Axin–adenomatous Polyposis Coli Interaction. *EMBO J* **19**:2270-2279 https://doi.org/10.1093/emboj/19.10.2270 | PubMed

39. **De Rycker M,** Price CM (2004) Tankyrase Polymerization Is Controlled by Its Sterile Alpha Motif and Poly(ADP-Ribose) Polymerase Domains. *Mol. Cell Biol* **24**:J9812 https://doi.org/10.1128/mcb.24.22.9802-9812.2004 | PubMed

40. **Pillay N,** Mariotti L, Zaleska M, Inian O, Jessop M, Hibbs S, Desfosses A, Hopkins PCR, Templeton CM, Beuron F, *et al.* (2022) Structural Basis of Tankyrase Activation by Polymerization. *Nature* **612**:162-169 https://doi.org/10.1038/s41586-022-05449-8 | PubMed

41. **Schwarz-Romond T,** Metcalfe C, Bienz M (2007) Dynamic Recruitment of Axin by Dishevelled Protein Assemblies. *J. Cell Sci* **120**:2402-2412 https://doi.org/10.1242/jcs.002956 | PubMed

42. **Nong J,** Kang K, Shi Q, Zhu X, Tao Q, Chen Y.-G (2021) Phase Separation of Axin Organizes the β-catenin Destruction Complex. *J. Cell Biol* **220**:e202012112 https://doi.org/10.1083/jcb.202012112 | PubMed

43. **Dow LE,** O'Rourke KP, Simon J, Tschaharganeh DF, van Es JH, Clevers H, Lowe SW (2015) Apc Restoration Promotes Cellular Differentiation and Reestablishes Crypt Homeostasis in Colorectal Cancer. *Cell* **161**:1539-1552 https://doi.org/10.1016/j.cell.2015.05.033 | PubMed

44. **Mygland L,** Brinch SA, Strand MF, Olsen PA, Aizenshtadt A, Lund K, Solberg NT, Lycke M, Thorvaldsen TE, Espada S, *et al.* (2021) Identification of Response Signatures for Tankyrase Inhibitor Treatment in tumor Cell Lines. *iScience* **24**:102807 https://doi.org/10.1016/j.isci.2021.102807 | PubMed

45. **Matyskiela ME,** Lu G, Ito T, Lu BPC.-C, Miller K, Fang W, Wang N.-Y, Nguyen D, Houston J, Carmel G, *et al.* (2016) A Novel Cereblon Modulator Recruits GSPT1 to the $CRL4^{CRBN}$ Ubiquitin Ligase. *Nature* **535**:252-257 https://doi.org/10.1038/nature18611 | PubMed

46. **Baradaran-Heravi A,** Balgi AD, Hosseini-Farahabadi S, Choi K, Has C, Roberge M (2021) Effect of Small Molecule eRF3 Degraders on Premature Termination Codon Readthrough. *Nucleic Acids Res* **49**:3692-3708 https://doi.org/10.1093/nar/gkab194 | PubMed

47. **Sellar RS,** Słabicki ASSM, Gasser JA, McConkey ME, Donovan KA, Mageed N, Adams DN, Zou C, Dutta PGMRK, Boettcher S, *et al.* (2022) Degradation of GSPT1 Causes TP53-independent Cell Death in Leukemia while Sparing Normal Hematopoietic Stem Cells. *J. Clin. Invest* **132**:e153514 https://doi.org/10.1172/jci153514 | PubMed

48. **Li N,** Zhang Y, Han X, Liang K, Wang J, Feng L, Wang W, Songyang Z, Lin C, Yang L, *et al.* (2015) Poly-ADP Ribosylation of PTEN by Tankyrases Promotes PTEN Degradation and Tumor Growth. *Genes Dev* **29**:157-170 https://doi.org/10.1101/gad.251785.114 | PubMed

49. **Morin PJ,** Vogelstein B, Kinzler KW (1996) Apoptosis and APC in Colorectal Tumorigenesis. *Proc. Natl. Acad. Sci* **93**:7950-7954 https://doi.org/10.1073/pnas.93.15.7950 | PubMed

50. **Schaefer KN,** Bonello TT, Zhang S, Williams CE, Roberts DM, McKay DJ, Peifer M (2018) Supramolecular Assembly of the beta-Catenin Destruction Complex and the Effect of Wnt Signaling on Its Localization, Molecular Size, and Activity In Vivo. *PLoS Genet* **14**:e1007339 https://doi.org/10.1371/journal.pgen.1007339 | PubMed

51. **Pronobis MI,** Rusan NM, Peifer M (2015) A Novel GSK3-regulated APC:Axin Interaction Regulates Wnt Signaling by Driving a Catalytic Cycle of Efficient β-catenin Destruction. *eLife* **4**:e08022 https://doi.org/10.7554/eLife.08022 | PubMed

52. **Bernkopf DB,** Brückner M, Hadjihannas MV, Behrens J (2019) An Aggregon in Conductin/axin2 Regulates Wnt/β-catenin Signaling and Holds Potential for Cancer Therapy. *Nat. Commun* **10**:4251 https://doi.org/10.1038/s41467-019-12203-8 | PubMed

53. **Schwarz-Romond T,** Fiedler M, Shibata N, Butler PJG, Kikuchi A, Higuchi Y, Bienz M (2007) The DIX Domain of Dishevelled Confers Wnt Signaling by Dynamic Polymerization. *Nat. Struct. Mol. Biol* **14**:484-492 https://doi.org/10.1038/nsmb1247 | PubMed

54. **Bischoff JR,** Anderson L, Zhu Y, Mossie K, Ng L, Souza B, Schryver B, Flanagan P, Clairvoyant F, Ginther C, *et al.* (1998) A Homologue of Drosophila Aurora Kinase Is Oncogenic and Amplified in Human Colorectal Cancers. *EMBO J* **17**:3052-3065 https://doi.org/10.1093/emboj/17.11.3052 | PubMed

55. **Dauch D,** Rudalska R, Cossa G, Nault J.-C, Kang T.-W, Wuestefeld T, Hohmeyer A, Imbeaud S, Yevsa T, Hoenicke L, *et al.* (2016) A MYC–aurora Kinase A Protein Complex Represents An Actionable Drug Target in p53-altered Liver Cancer. *Nat. Med* **22**:744-753 https://doi.org/10.1038/nm.4107 | PubMed

56. **Menon M,** Elliott R, Bowers L, Balan N, Rafiq R, Costa-Cabral S, Munkonge F, Trinidade I, Porter R, Campbell AD, *et al.* (2019) A Novel Tankyrase Inhibitor, MSC2504877, Enhances the Effects of Clinical CDK4/6 Inhibitors. *Sci. Rep.* **9**:201 https://doi.org/10.1038/s41598-018-36447-4 | PubMed

57. **Foronda M,** Tarumoto Y, Schatoff EM, Leach BI, Diaz BJ, Zimmerman J, Goswami S, Shusterman M, Vakoc CR, Dow LE (2019) Tankyrase Inhibition Sensitizes Cells to CDK4 Blockade. *PLoS One* **14**:e0226645 https://doi.org/10.1371/journal.pone.0226645 | PubMed

58. **Wang H,** Lu B, Castillo J, Zhang Y, Yang Z, McAllister G, Lindeman A, Reece-Hoyes J, Tallarico J, Russ C, *et al.* (2016) Tankyrase Inhibitor Sensitizes Lung Cancer Cells to Endothelial Growth Factor Receptor (EGFR) Inhibition via Stabilizing Angiomotins and Inhibiting YAP Signaling. *J. Biol. Chem* **291**:15256-15266 https://doi.org/10.1074/jbc.m116.722967 | PubMed

59. **Schoumacher M,** Hurov KE, Lehár J, Yan-Neale Y, Mishina Y, Sonkin D, Korn JM, Flemming D, Jones MD, Antonakos B, *et al.* (2014) Inhibiting Tankyrases Sensitizes KRAS-Mutant Cancer Cells to MEK Inhibitors via FGFR2 Feedback Signaling. *Cancer Res* **74**:3294-3305 https://doi.org/10.1158/0008-5472.can-14-0138-t | PubMed

60. **Zhong Y,** Katavolos P, Nguyen T, Lau T, Boggs J, Sambrone A, Kan D, Merchant M, Harstad E, Diaz D, *et al.* (2016) Tankyrase Inhibition Causes Reversible Intestinal Toxicity in Mice with a Therapeutic Index < 1. *Toxicol Pathol* **44**:267-278 https://doi.org/10.1177/0192623315621192 | PubMed

61. **Norum JH,** Skarpen E, Brech A, Kuiper R, Waaler J, Krauss S, Sørlie T (2018) The Tankyrase Inhibitor G0071ZLK Inhibits Small Intestine LGR5+ Stem Cell Proliferation Without Altering Tissue Morphology. *Biol. Res* **51**:3 https://doi.org/10.1186/s40659-017-0151-6 | PubMed

62. **Zhong L,** Ding Y, Bandyopadhyay G, Waaler J, Börgeson E, Smith S, Zhang M, Phillips SA, Mahooti S, Mahata SK, *et al.* (2016) The PARsylation Activity of Tankyrase in Adipose Tissue Modulates Systemic Glucose Metabolism in Mice. *Diabetologia* **59**:582-591 https://doi.org/10.1007/s00125-015-3815-1 | PubMed

63. **Tian H,** Biehs B, Warming S, Leong KG, Rangell L, Klein OD, de Sauvage FJ (2011) A Reserve Stem Cell Population in Small Intestine Renders *Lgr5*-positive Cells Dispensable. *Nature* **478**:255-259 https://doi.org/10.1038/nature10408 | PubMed

64. **Lieu CH,** Lenz H.-J, Benson AB, Meng X, Kim U.-I, Kim SH, Kim K, Sung MJ (2025) A First-In-Human Dose-Escalation Phase I Study of Basroparib, a Tankyrase Inhibitor, in Patients with Advanced-Stage Solid Tumors. *Cancer Res Commun* **5**:1771-1778 https://doi.org/10.1158/2767-9764.crc-25-0502 | PubMed

65. **Langelier M.-F,** Zandarashvili L, Aguiar PM, Black BE, Pascal JM (2018) NAD^+ Analog Reveals PARP-1 Substrate-blocking Mechanism and Allosteric Communication from Catalytic Center to DNA-binding Domains. *Nat. Commun* **9**:844 https://doi.org/10.1038/s41467-018-03234-8 | PubMed

66. **Pollock K,** Liu M, Zaleska M, Meniconi M, Pfuhl M, Collins I, Guettler S (2019) Fragment-based Screening Identifies Molecules Targeting the Substrate-binding Ankyrin Repeat Domains of Tankyrase. *Sci. Rep* **9**:19130 https://doi.org/10.1038/s41598-019-55240-5 | PubMed

67. **Sowa ST,** Vela-Rodríguez C, Galera-Prat A, Cázares-Olivera M, Prunskaite-Hyyryläinen R, Ignatev A, Lehtiö L (2020) A FRET-based High-throughput Screening Platform for the Discovery of Chemical Probes Targeting the Scaffolding Functions of Human Tankyrases. *Sci. Rep* **10**:12357 https://doi.org/10.1038/s41598-020-69229-y | PubMed

68. **Wang J,** Mouradov D, Wang X, Jorissen RN, Chambers MC, Zimmerman LJ, Vasaikar S, Love CG, Li S, Lowes K, *et al.* (2017) Colorectal Cancer Cell Line Proteomes Are Representative of Primary Tumors and Predict Drug Sensitivity. *Gastroenterology* **153**:1082-1095 https://doi.org/10.1053/j.gastro.2017.06.008 | PubMed

69. **Semenova E,** Guerriero M.-L, Zhang B, Hock A, Hopcroft P, Kadamur G, Afzal AM, Lazic SE (2021) Flexible Fitting of PROTAC Concentration-Response Curves with Changepoint Gaussian Processes. *SLAS Discov* **26**:1212-1224 https://doi.org/10.1177/24725552211028142 | PubMed

70. **Steinebach C,** Sosic I, Lindner S, Bricelj A, Kohl F, Ng YLD, Monschke M, Wagner KG, Kroenke J, Guetschow M (2019) A MedChem Toolbox for Cereblon-directed PROTACs. *MedChemComm* **10**:1037-1041 https://doi.org/10.1039/c9md00185a | PubMed

71. **Zhang L.-s,** Kang X, Lu J, Zhang Y, Wu X, Wu G, Zheng J, Tuladhar R, Shi H, Wang Q, *et al.* (2019) Installation of a Cancer Promoting WNT/SIX1 Signaling Axis by the Oncofusion Protein MLL-AF9. *EBioMedicine* **39**:145-158 https://doi.org/10.1016/j.ebiom.2018.11.039 | PubMed

72. **Bond MJ,** Chu L, Nalawansha DA, Li K, Crews CM (2020) Targeted Degradation of Oncogenic KRAS^{G12C} by VHL-Recruiting PROTACs. *ACS Cent Sci* **6**:1367-1375 https://doi.org/10.1021/acscentsci.0c00411 | PubMed

73. **Hrast M,** Rožman K, Jukič M, Patin D, Gobec S, Sova M (2017) Synthesis and Structure–activity Relationship Study of Novel Quinazolinone-based Inhibitors of MurA. *Bioorg Med Chem Lett* **27**:3529-3533 https://doi.org/10.1016/j.bmcl.2017.05.064 | PubMed

74. **Li Y,** Yang J, Aguilar A, McEachern D, Przybranowski S, Liu L, Yang C.-Y, Wang M, Han X, Wang S (2019) Discovery of MD-224 as a First-in-Class, Highly Potent, and Efficacious Proteolysis Targeting Chimera Murine Double Minute 2 Degrader Capable of Achieving Complete and Durable Tumor Regression. *J. Med. Chem.* **62**:448-466 https://doi.org/10.1021/acs.jmedchem.8b00909 | PubMed

75. **Kang S,** Kim YM, Kim RY, Seo MJ, No Z, Nam K, Kim S, Kim J (2017) Synthesis and Structure-activity Studies of Side Chain Analogues of the Anti-tubercular Agent, Q203. *Eur. J. Med. Chem.* **125**:807-815 https://doi.org/10.1016/j.ejmech.2016.09.082 | PubMed

76. **Hansen JD,** Correa M, Nagy MA, Alexander M, Plantevin V, Grant V, Whitefield B, Huang D, Kercher T, Harris R, *et al.* (2020) Discovery of CRBN E3 Ligase Modulator CC-92480 for the Treatment of Relapsed and Refractory Multiple Myeloma. *J. Med. Chem* **63**:6648-6676 https://doi.org/10.1021/acs.jmedchem.9b01928 | PubMed

77. **Dwight SJ,** Levin S (2016) Scalable Regioselective Synthesis of Rhodamine Dyes. *Org Lett* **18**:5316-5319 https://doi.org/10.1021/acs.orglett.6b02635 | PubMed

Chen C (2022) Tankyrase-induced liquid-to-solid phase transition hinders beta-catenin degradation. MassIVE. ID MSV000089098 https://massive.ucsd.edu/ProteoSAFe/dataset.jsp?accession=MSV000089098

Peer reviews

Reviewer #1 (Public review):

Summary:

This manuscript reports the discovery and characterization of the first bifunctional degrader of tankyrase. Notably, the tankyrase degrader exhibits stronger β-catenin inhibition and tumor growth suppression compared to conventional tankyrase inhibitors. Mechanistically, while tankyrase inhibitors stabilize tankyrase and promote Axin puncta formation-thereby impairing β-catenin degradation-the degrader avoids this effect, resulting in deeper suppression of β-catenin signaling. These findings suggest that targeted degradation of tankyrase offers a novel therapeutic strategy for β-catenin-driven cancers. Overall, this is a compelling study with significant translational potential.

Strengths:

(1) The manuscript presents a rigorous and well-executed study on a timely and impactful topic.

(2) The biochemical and cellular characterization of the tankyrase degrader is thorough, and the comparative analysis with tankyrase inhibitors is insightful.

(3) The finding that tankyrase stabilization by inhibitors may interfere with Axin function is novel and significant. It aligns with earlier observations (e.g., Huang 2009) that transient tankyrase overexpression can stabilize β-catenin independently of PAR domain activity.

(4) The use of TNKS1/2 knockout cells expressing catalytically inactive tankyrase to demonstrate β-catenin inhibitory activity of the tankyrase degrader is elegant.

(5) The finding that the tankyrase degrader has superior anti-proliferative effects in colorectal cancer models has important therapeutic implications.

Comments on revised version:

I had a favorable opinion of the manuscript in the first round of review. I don't have additional comments on the revised manuscript. The manuscript looks fine to me.

https://doi.org/10.7554/eLife.109052.2.sa4

Reviewer #2 (Public review):

Summary:

The ADP-ribosyltransferase tankyrase controls many biological processes, many of which are relevant to human disease. This includes Wnt/beta-catenin signalling, which is dysregulated in many cancers, most notably colorectal cancer. Tankyrase is a positive regulator of Wnt/beta-catenin signalling in that it counters the activity of the beta-catenin destruction complex (DC). Catalytic inhibition of tankyrase not only blocks PAR-dependent ubiquitylation and degradation of AXIN1/2, the central scaffolding protein in the DC, but also tankyrase itself. As a result, blocking tankyrase gives rise to tankyrase accumulation, which may accentuate its non-catalytic functions, which have been proposed to drive Wnt/beta-catenin signalling. Most tankyrase catalytic inhibitors have shown limited efficacy and substantial toxicity in vivo. By developing tankyrase-directed PROTACs, the authors aim to block both catalytic and non-catalytic functions of tankyrase, aspiring to achieve a more complete inhibition of Wnt/beta-catenin signalling. The successfully developed PROTAC, based on the existing catalytic inhibitor IWR1, IWR1-POMA, induces the degradation of both TNKS and TNKS2, blocks beta-catenin-dependent transcription without stabilising the DC in puncta/degradasomes, and inhibits cancer cell growth in vitro. Mechanistically, this points to a scaffolding role of tankyrase in the DC, at least under conditions of tankyrase catalytic inhibition, in line with previous proposals.

Strengths:

The study clearly illustrates the incentive for developing a tankyrase degrader, namely, to abolish both catalytic and non-catalytic functions of tankyrase. By and large, the study achieves these ambitions, and the findings support the main conclusions, although the statement that a more complete inhibition of the pathway is achieved requires corroboration. The proteomics studies are powerful. IWR1-POMA constitutes a very useful tool to re-evaluate targeting of tankyrase in oncogenic Wnt/beta-catenin signalling. The paired compounds will benefit investigations of tankyrase scaffolding functions across many different biological systems controlled by tankyrase. The findings are exciting.

Comments on revised version:

I thank the authors for responding to the queries raised in the original review, most of which have now been addressed. This further strengthens this well-conducted study and well-presented manuscript. I congratulate the authors for this interesting and insightful work.

A few minor points remain:

I appreciate the authors acknowledge that testing the physical properties of the degradasome puncta is necessary to explore whether they indeed represent condensates. The term "condensates" implies liquid-liquid phase separation (rightly or wrongly). However, this question has not yet been resolved in the case of degradasomes. I therefore suggest the term "condensates" to be avoided. A simple morphological description as "puncta" may suffice.

I thank the authors for including the additional data comparing tankyrase binding by IWR and IWR-POMA. I agree that using the BRET signal of IWR-POMA is informative. Adding the IC50 values directly to the figure panels (S3E, S3G) would help the reader to quickly assess binding. The comparison between these two panels is insightful.

Regarding the use of the terms TNKS, TNKS1 and TNKS2, if the authors would like to use the name "TNKS" to refer to both paralogues collectively, can this please be specified early in the manuscript to limit confusion with the official gene name "TNKS", which of course only refers to one paralogue?

https://doi.org/10.7554/eLife.109052.2.sa3

Reviewer #3 (Public review):

In this manuscript, Wang et al employ a chemical biology approach to investigate the differences between the enzymatic and scaffolding roles of tankyrase during Wnt β-catenin signalling. It was previously established that, in addition to its enzymatic activity, tankyrase 1/2 also plays a scaffolding function within the destruction complex, a property conferred by SAM-domain-dependent polymerization (PMID: 27494558). It is also known that TNKS1/2 is an autoregulated protein and that its enzymatic inhibition leads to accumulation of total TNKS proteins and stabilization of Axin punctae (through the scaffolding function of TNKS1/2), leading to rigidification of the DC and decreased β-catenin turnover. The authors surmised that this could, in part, explain the limited efficacy of TNKS1/2 catalytic inhibition for the treatment of colorectal cancers. To test this hypothesis, they evaluated a series of PROTAC molecules promoting the degradation of TNKS1/2 to block both the catalytic and scaffolding activities. They show that IWR1-POMA (their most active molecule) promotes more efficient suppression of beta-catenin-mediated transcription and is more active in inhibiting colorectal cancer cell and CRC patient-derived organoids growth. Mechanistically, the authors used FRAP to demonstrate that catalytic inhibitors of TNKS led to a reduced dynamic assembly of the DC (rigidification), whereas IWR1-POMA did not affect the dynamics.

Overall, this is an interesting study describing the design and development of a PROTAC for TNKS1/2 that could have increased efficacy where catalytic inhibitors have displayed limited activity. Knowing the importance of the scaffolding role of TNKS1/2 within the destruction complex, targeting both the catalytic and scaffolding roles certainly makes sense. The manuscript contains convincing evidence of the different mechanisms of the PROTAC vs catalytic inhibitors. Some additional efforts to quantify several of the experiments and to indicate the reproducibility and statistical analysis would strengthen the manuscript. Ultimately, it would have been great to evaluate the in vivo efficacy of IWR1-POMA in an in vivo CRC assay (APCmin mice or using PDX models); however, I realize that this is likely beyond the scope of this manuscript.

https://doi.org/10.7554/eLife.109052.2.sa2

Reviewer #4 (Public review):

From the Reviewing Editor:

This important study reports the development of the first PROTACs targeting the ADP-ribosyltransferases tankyrase 1 and 2, with the goal of inhibiting Wnt/β-catenin signaling more completely than is possible with catalytic tankyrase inhibitors. The work addresses a significant limitation of existing tankyrase inhibitors: although catalytic inhibition stabilizes AXIN1/2 and suppresses Wnt signaling, it also stabilizes tankyrase itself, potentially enhancing non-catalytic scaffolding functions and promoting accumulation of degradasome-like puncta.

The evidence is convincing. The authors use appropriate and well-validated approaches, including chemical biology, cellular assays, and proteomic profiling, to show that PROTAC-mediated degradation of tankyrase avoids tankyrase accumulation while still stabilizing AXIN and inhibiting Wnt/β-catenin signaling. The data support the conclusion that degradation of tankyrase can separate pathway inhibition from the confounding effects of stabilized tankyrase protein and may therefore offer advantages over conventional catalytic inhibitors.

A strength of the study is the clear mechanistic comparison between tankyrase degradation and catalytic inhibition. The manuscript provides convincing evidence that the PROTAC and catalytic inhibitors act through distinct mechanisms, with the PROTAC targeting both catalytic and scaffolding roles of tankyrase. The study is well conducted and clearly presented, and the authors have addressed most concerns raised during review.

A remaining limitation is that the therapeutic potential of the compound is not tested in vivo, for example in APC-mutant colorectal cancer models, APCmin mice, or patient-derived xenografts. Such experiments would strengthen claims about practical efficacy, although they are not essential for the main mechanistic conclusions of the manuscript.

Overall, this is an important and insightful contribution. It advances the tankyrase and Wnt signaling fields by providing a new chemical strategy to suppress tankyrase function more completely than catalytic inhibition alone, and it offers a useful framework for future therapeutic exploration of tankyrase degradation.

https://doi.org/10.7554/eLife.109052.2.sa1

Author response:

The following is the authors' response to the original reviews.

> ***Public Reviews:***
>
> ***Reviewer #1 (Public review):***
>
> *Summary:*
>
> *This manuscript reports the discovery and characterization of the first bifunctional degrader of tankyrase. Notably, the tankyrase degrader exhibits stronger β-catenin inhibition and tumor growth suppression compared to conventional tankyrase inhibitors. Mechanistically, while tankyrase inhibitors stabilize tankyrase and promote Axin puncta formation - thereby impairing β-catenin degradation - the degrader avoids this effect, resulting in deeper suppression of β-catenin signaling. These findings suggest that targeted degradation of tankyrase offers a novel therapeutic strategy for β-catenin-driven cancers. Overall, this is a compelling study with significant translational potential.*
>
> *Strengths:*

(1) The manuscript presents a rigorous and well-executed study on a timely and impactful topic.

(2) The biochemical and cellular characterization of the tankyrase degrader is thorough, and the comparative analysis with tankyrase inhibitors is insightful.

(3) The finding that tankyrase stabilization by inhibitors may interfere with Axin function is novel and significant. It aligns with earlier observations (e.g., Huang 2009) that transient tankyrase overexpression can stabilize β-catenin independently of PAR domain activity.

(4) The use of TNKS1/2 knockout cells expressing catalytically inactive tankyrase to demonstrate β-catenin inhibitory activity of the tankyrase degrader is elegant.

(5) The finding that the tankyrase degrader has superior anti-proliferative effects in colorectal cancer models has important therapeutic implications.

Weaknesses:

(1) A key caveat is that the identified tankyrase degrader also targets GSPT1 for degradation. This raises the possibility that GSPT1 degradation may contribute to the observed β-catenin and tumor growth inhibition.

(2) The authors address this concern reasonably by showing that DLD1 cells resistant to GSPT1 degradation remain sensitive to the tankyrase degraded.

(3) To further strengthen this point, the authors might consider generating TNKS1/2 double knockout cells (e.g., in DLD1 or SW480 backgrounds) and demonstrating that the degrader loses its growth-inhibitory effect in these models. However, given the technical challenges of creating double knockouts in cancer cell lines, such experiments could be considered optional.

We thank the Reviewer for the favorable feedback. The major concern is the collateral degradation of GSPT1. As the Reviewer noted, IWR1-POMA was able to suppress colony formation in DLD-1 cells resistant to a GSPT1/2 degrader (DLD-1R, Figure 6B and S9F), suggesting that TNKS but not GSPT degradation is responsible for growth inhibition.

We also appreciate that the Reviewer brought it to our attention an important early observation of the TNKS scaffolding effects. Cong reported in 2009 that overexpression of TNKS induced AXIN puncta formation in a SAM but not PARP domain-dependent manner (PMID: 19759537, Ref. 12). We have added this reference to the introduction of TNKS scaffolding in the revised manuscript.

Reviewer #2 (Public review):

Summary:

The ADP-ribosyltransferase tankyrase controls many biological processes, many of which are relevant to human disease. This includes Wnt/beta-catenin signalling, which is dysregulated in many cancers, most notably colorectal cancer. Tankyrase is a positive regulator of Wnt/beta-catenin signalling in that it counters the activity of the beta-catenin destruction complex (DC). Catalytic inhibition of tankyrase not only blocks PAR-dependent ubiquitylation and degradation of AXIN1/2, the central scaffolding protein in the DC, but also tankyrase itself. As a result, blocking tankyrase gives rise to tankyrase accumulation, which may accentuate its non-catalytic functions, which have been proposed to drive Wnt/beta-catenin signalling. Most tankyrase catalytic inhibitors have shown limited efficacy and substantial toxicity in vivo. By developing tankyrase-directed

> *PROTACs, the authors aim to block both catalytic and non-catalytic functions of tankyrase, aspiring to achieve a more complete inhibition of Wnt/beta-catenin signalling. The successfully developed PROTAC, based on the existing catalytic inhibitor IWR1, IWR1-POMA, induces the degradation of both TNKS and TNKS2, blocks beta-catenin-dependent transcription without stabilising the DC in puncta/degradasomes, and inhibits cancer cell growth in vitro. Mechanistically, this points to a scaffolding role of tankyrase in the DC, at least under conditions of tankyrase catalytic inhibition, in line with previous proposals.*
>
> *Strengths:*
>
> *The study clearly illustrates the incentive for developing a tankyrase degrader, namely, to abolish both catalytic and non-catalytic functions of tankyrase. By and large, the study achieves these ambitions, and the findings support the main conclusions, although the statement that a more complete inhibition of the pathway is achieved requires corroboration. The proteomics studies are powerful. IWR1-POMA constitutes a very useful tool to re-evaluate targeting of tankyrase in oncogenic Wnt/beta-catenin signalling. The paired compounds will benefit investigations of tankyrase scaffolding functions across many different biological systems controlled by tankyrase. The findings are exciting.*
>
> *Weaknesses:*
>
> *Although the results are promising and mostly compelling, the claim that the PROTACs provide "a deeper suppression of the WNT/β-catenin pathway activity" requires further corroboration, particularly at endogenous tankyrase levels.*

We thank the Reviewer for the encouraging and insightful comments. The major critique concerns whether TNKS degraders can suppress WNT/β-catenin signaling more effectively than TNKS inhibitors at endogenous TNKS levels. IWR1-POMA reduced the level of cytosolic β-catenin more effectively than IWR1 in Wnt3A-stimulated HEK293 cells without protein overexpression (Figure 1D). IWR1POMA also suppressed STF activity more effectively than IWR1 in DLD-1 cells (Figure S8C) and reduced the expression levels of several WNT/β-catenin targets more effectively than IWR1 (Figure 1G and S8D). These results support that TNKS degraders can suppress WNT/β-catenin signaling more effectively than TNKS inhibitors at endogenous TNKS levels.

> *There are also some other points that, if considered, would further improve the manuscript, as detailed below.*
>
> *(1) Abstract and line 62: Many catalytic tankyrase inhibitors tend to display toxicity, which is likely on-target (e.g., 10.1177/0192623315621192; 10.1158/0008-5472). This constitutes the main limiting factor for these compounds. An incomplete inhibition of Wnt/beta-catenin signalling may contribute to the challenges, but this does not appear to be the dominant problem. A more prominent introduction to this important challenge is probably expected by the field.*

A previous study showed that G007-LK, a selective TNKS inhibitor, exhibited weak efficacy and dose-limiting toxicity at 5–30 mg/kg BID or 10–60 mg/kg QD in various mouse xenograft models (PMID: 23539443, Ref. 28). Similarly, G-631, another TNKS inhibitor, also showed dose-limiting toxicity without significant efficacy at 25–100 mg/kg QD in mice (PMID: 26692561, Ref. 60). However, other studies showed that G007-LK was well-tolerated at 200 mg/kg QD over 3 weeks in mice (PMID: 29316982, Ref. 61), and treating mice with G007-LK at 10 mg/kg QD over 6 months also improved glucose tolerance without notable toxicity (PMID: 26631215, Ref. 62). Importantly, basroparib, a selective TNKS inhibitor, was well tolerated in a recent clinical trial (PMID: 40964966, Ref. 64), and constitutive silencing of both TNKS1 and TNKS2 for 150 days in APC-null mice prevented tumorigenesis without damaging the intestines (PMID: 31337618, Ref. 8). We have included some discussion of the toxicity issue associated with TNKS targeting at the end of the Discussion section.

> *(2) The authors do a good job in setting the scene for the need for tankyrase degraders. Their observations relating to the formation of puncta (degradasomes) being tankyrase-dependent are compatible with a previous study by Martino-Echarri et al. 2016 (10.1371/journal.pone.0150484): simultaneous silencing of TNKS and TNKS2 by RNAi abolishes degradasome formation. The paper is cited as reference 17, but only in passing, and deserves more prominence. (It includes an entire paragraph titled "Expression of tankyrases 1 and 2 is required for TNKSi-induced formation of axin puncta").*

Indeed, Henderson's 2016 paper (PMID: 26930278, previously Ref. 17, now Ref. 18) shed important light on the role of TNKS scaffolding in the DC. However, whereas this study demonstrated that knocking down both TNKS1 and TNKS2 by siRNA prevented G007-LK to induce AXIN puncta, it concluded that "puncta formation requires both the expression and the inactivation of TNKS," which is inconsistent with our observations that accumulation of either catalytically active or inactive TNKS can promote AXIN puncta formation. The function roles of TNKS scaffolding in the DC also remained unaddressed. We have included additional discussion of Henderson's findings in the first paragraph the Discussion section.

> *(3) Moreover, the scaffolding concept has been discussed comprehensively in other studies: 10.1111/bph.14038 and more recently 10.1042/BCJ20230230. There are also a few studies that focus on targeting the ankyrin repeat clusters of tankyrase to disengage substrates (10.1038/s41598-020-69229-y; 10.1038/s41598-019-55240-5) that illustrate the concept of blocking the scaffolding function. In that sense, the hypotheses are mature, and it is interesting to see some of them supported in this study. The authors could improve how they set their work into the context of these other efforts and proposals.*

Indeed, Guettler demonstrated in 2016 that TNKS scaffolding could promote WNT/β-catenin signaling, which forms the basis of the current work. Meanwhile, whereas there have been efforts to target the SAM or ARC domain to address TNKS scaffolding by Guettler and Lehtiö, our approach of targeting TNKS for degradation is complementary. We have included in the last paragraph of the Discussion section information on efforts to target the ARC or SAM domains as an alternative approach to suppress WNT/β-catenin signaling without promoting TNKS oligomerization (PMID: 31836723 and 32704068, Ref. 66 and 67).

> *(4) In several places in the manuscript, the DC is referred to as "biomolecular condensate", at times even as a "classic example", implying that it operates through phase separation. This has not been demonstrated. In fact, super-resolution microscopy indicates that the puncta are not droplet-like (10.7554/eLife.08022), which would argue against the condensate hypothesis.*

Biomolecular condensates are membraneless cellular compartments formed by phase separation of biomolecules, regardless of their physical/material properties (PMID: 28935776 and 28225081, Ref. 22 and 23). Super-resolution microscopy studies by Stenmark (PMID: 26124443, Ref. 17) showed that AXIN, APC, TNKS, and β-catenin interacted with each other to assemble into membraneless complexes, wherein AXIN and APC formed filaments throughout the DC. Peifer has also summarized evidence that supports the condensate nature of the DC (PMID: 30782412, Ref. 9; see also PMID: 26393419). However, we acknowledge that testing the physical properties of reconstituted DC (for example, PMID: 34352208) with TNKS will provide a better understanding of the nature, for example liquid vs. gel, of these condensates.

> *(5) It is beautiful to be able to use IWR1 and IWR1-POMA at identical concentrations for direct comparisons. However, this requires the two compounds to bind to tankyrase similarly well and reach the target to a comparable extent. How sure are authors that target engagement is comparable? Has this been evaluated?*

Using a BRET assay, we have confirmed that IWR1-POMA binds to TNKS1 with affinity comparable to that of IWR1. Details of this study is now included in the Results sections, and the data are presented in the Supplementary Information (Fig. S3E–G).

> *(6) Figure 1F: It is not immediately apparent how IWR1-POMA shows more complete containment of Wnt/beta-catenin signalling. Most Wnt/beta-catenin targets lie close to the perfect diagonal, so I do not see how the statement "that IWR1-POMA controlled WNT/β-catenin signaling more effectively than IWR1" (in the legend of Figure 1F) is supported. Minimally, an expanded explanation would benefit the reader. Providing the colour-coding legend directly in the figure would help improve clarity. Also, the panel is very small and may benefit from a different presentation in the figure.*

We have updated Fig. 1F to include an inset of Quadrant III for improved clarity and readability. We have also moved Fig. S7C to the main text as Fig. 1G and added an expanded explanation for these figures.

> *(7) Figure 2: The conclusion of a "deeper suppression" of signalling relies on overexpression of tankyrase in an otherwise tankyrase-null background. Have the authors attempted to measure reporter activity or endogenous gene expression without tankyrase overexpression, in Wnt3a-stimulated cells (in the context of a normal Wnt/beta-catenin pathway) or CRC cells at the basal level? Non-catalytic activity in a similar assay has previously been observed upon tankyrase overexpression (10.1016/j.molcel.2016.06.019). Whether or not there is a substantial scaffolding effect at endogenous tankyrase levels after tankyrase inhibition remains unconfirmed, and the PROTAC is a valuable tool to address this important question. The findings presented in Figure S7C and D go some way towards answering this question - these data could be presented more prominently, and similar assays could be performed in other cell systems.*

IWR1-POMA suppressed STF activity more effectively than IWR1 in *APC*-mut DLD-1 and SW480 CRC cells without TNKS overexpression (Fig. S8C). Similarly, IWR1-POMA provided a deeper suppression of STF signals in HeLa cells transfected with AXIN1 and β-catenin while expressing endogenous TNKS (Fig. 4G). These results suggest that inhibitor-induced TNKS scaffolding plays a significant role at endogenous TNKS expression levels. Following the reviewer's suggestion, Fig. S7C is now Fig. 1G.

> *(8) Line 237/238: "TNKS accumulation negatively impacts the catalytic activity of the DC (Figure 5D)" - the data do not show this. Beta-catenin levels are a surrogate readout for DC function (phosphorylation and ubiquitylation). Minimally, this requires rewording, with reference to beta-catenin levels.*

We have rephrased "TNKS accumulation negatively impacts the catalytic activity of the DC" as "TNKS accumulation negatively impacts the exchange of β-catenin in the DC."

> *(9) Line 303-304: Beta-catenin is thought to exchange at beta-catenin degradasomes; this is clear from previous FRAP assays and the observation that phospho-beta-catenin accumulates in degradasomes upon proteasome inhibition (10.1158/1541-7786.MCR-15-0125). However, degradasome size hasn't, to my knowledge, been related to activity. Can this be clarified, please?*

We apologize for confusing β-catenin phosphorylation with β-catenin abundance. Here, we refer the catalytic activity of the DC to as the ability of the DC to promote β-catenin degradation rather than the kinetics of β-catenin phosphorylation. It is commonly observed that AXIN stabilization by TNKS inhibitors increases the DC size and reduces the β-catenin levels. As such, the induction of AXIN puncta by TNKS inhibitors is frequently used as an indicator of WNT/β-catenin pathway inhibition. However, we have found that, TNKS inhibition drives TNKS accumulation, which reduces the ability of the DC to promote β-catenin degradation. We agree that the DC only primes β-catenin but does not catalyze its degradation. We have revised our manuscript as follows: "increasing the local concentration of the DC components improves its 'effective activity'[50,51]."

> *(10) There are previous hypotheses/proposals that the sensitivity of CRC cells to tankyrase inhibition correlates with APC truncation or PIK3CA status (10.1158/1535-7163.MCT-16-0578; 10.1038/s41416-023-02484-8). Have the authors considered expanding their cell line panel (Figure S7) to sample a wider range of cell lines, including some that are wild-type with regard to APC or Wnt/beta-catenin signalling in general? This would be a valuable addition to the work. Quantitated colony formation data could be moved to the main body of the manuscript.*

We have so far tested the effects of IWR1-POMA on the proliferation of DLD-1, SW480, HT-29, HCT116, and RKO cells (Fig. 6A and 6B). While a heterozygous Ser45 deletion in *CTNNB1* confers resistance to IWR1-POMA, we did not observe sensitivity associated with *APC* or *PIK3CA* status. The ability of IWR1-POMA to suppress the growth of RKO cells expressing wild-type APC is consistent with a previous report that knockdown of both TNKS1 and TNKS2 stabilized PTEN to suppress cell proliferation and glycolysis *in vitro* and tumor growth *in vivo* (PMID: 25547115, Ref. 48) independently of the β-catenin pathway. We have added this new information as well as quantification of the colony growth results (Fig. S8A, S8B, S9A, S9F, and S9G) to the revised manuscript.

> *(11) The manuscript only mentions toxicity (i.e., therapeutic window) in the last sentence of the Discussion section. As this is THE main challenge with tankyrase inhibitors (as mentioned above), can the authors expand their discussion of this aspect? Is there an expectation that PROTACs may be less toxic?*

As discussed above, evidence for on-target toxicity of WNT/β-catenin inhibition is mixed. Yet, the absence of dose-limiting toxicity for basroparib at doses up to 360 mg QD in human (PMID: 40964966, Ref. 64) is encouraging. PROTAC works by catalyzing target degradation, which is different from traditional catalytic inhibitors that require continuous target occupancy at a high level. It remains unclear whether the observed on-target toxicity of TNKSi is associated with TNKS accumulation at high doses, akin to the cytotoxicity induced by PARP1-trapping upon catalytic inhibition. We have included a brief discussion of the toxicity issue in the final paragraph of the Discussion section.

> *(12) Figures 3, 4, 5A: For fluorescence microscopy experiments, can these be quantified, and can repeat data be included?*

We have included quantification data and replicate information for Fig. 3–5.

> *(13) Figure 4, S6: An additional channel illustrating the distribution of cells (e.g., nuclei, cytoskeleton, or membrane) would be helpful for orientation and context for the AXIN1 signal.*

We have included cell outlines or nuclear staining for Fig. 3, 4, S6, and S7.

> *(14) How were cytosolic fractions of cells prepared to assess cytosolic beta-catenin levels? This detail is missing from the methods.*

We have updated the Methods section to include additional details on the preparation of the cytosolic fractions of cells.

> ***Reviewer #3 (Public review):***
>
> *In this manuscript, Wang et al employ a chemical biology approach to investigate the differences between the enzymatic and scaffolding roles of tankyrase during Wnt β-catenin signalling. It was previously established that, in addition to its enzymatic activity, tankyrase 1/2 also plays a scaffolding function within the destruction complex, a property conferred by SAM-domain-dependent polymerization (PMID: 27494558). It is also known that TNKS1/2 is an autoregulated protein and that its enzymatic inhibition leads to accumulation of total TNKS proteins and stabilization of Axin punctae (through the scaffolding function of TNKS1/2), leading to rigidification of the DC and decreased β-catenin turnover. The authors surmised that this could, in part, explain the limited efficacy of TNKS1/2 catalytic inhibition for the treatment of colorectal cancers. To test this hypothesis, they evaluated a series of PROTAC molecules promoting the degradation of TNKS1/2 to block both the catalytic and scaffolding activities. They show that IWR1-POMA (their most active molecule) promotes more efficient suppression of beta-catenin-mediated transcription and is more active in inhibiting colorectal cancer cell and CRC patient-derived organoids growth. Mechanistically, the authors used FRAP to demonstrate that catalytic inhibitors of TNKS led to a reduced dynamic assembly of the DC (rigidification), whereas IWR1-POMA did not affect the dynamics.*
>
> *Overall, this is an interesting study describing the design and development of a PROTAC for TNKS1/2 that could have increased efficacy where catalytic inhibitors have displayed limited activity. Knowing the importance of the scaffolding role of TNKS1/2 within the destruction complex, targeting both the catalytic and scaffolding roles certainly makes sense. The manuscript contains convincing evidence of the different mechanisms of the PROTAC vs catalytic inhibitors. Some additional efforts to quantify several of the experiments and to indicate the reproducibility and statistical analysis would strengthen the manuscript. Ultimately, it would have been great to evaluate the in vivo efficacy of IWR1-POMA in an in vivo CRC assay (APCmin mice or using PDX models); however, I realize that this is likely beyond the scope of this manuscript.*

We thank the Reviewer for the helpful suggestions.

> *I have some recommendations listed below for consideration by the authors to strengthen their study:*
>
> *(1) The title is slightly misleading, as it is already known that the scaffolding function of TNKS is important within the DC. The authors should consider incorporating the PROTAC targeting aspect in the title (e.g., PROTAC-mediated targeting of tankyrase leads to increased inhibition of betacat signaling and CRC growth inhibition).*

We have modified the title accordingly to "Targeting tankyrase scaffolding in the β-catenin destruction complex by PROTAC overcomes the limitation of catalytic inhibitors in cancer."

> *(2) The authors should comment in the manuscript on the bell-shaped curve obtained with treatment of cells with the PROTACs (Figure S2C). This likely indicates tittering of the targets within a bifunctional molecule with increasing concentration (and likely reveals the auto-inhibition conferred by the catalytic inhibition alone).*

As suggested by the Reviewer, the bell-shaped dose-response likely originated from the formation of non-productive binary protein-ligand complexes at high PROTAC concentrations. We have added a sentence to clarify this unique behavior of PROTAC molecules.

> *(3) The authors comment that using G007-LK as warehead was unsuccessful, but they do not show data. Do the authors know why this was the case?*

The structure-activity relationship of PROTACs is often unpredictable, as both the kinetics and thermodynamics of target and E3 ligase binding play important roles in promoting efficient target degradation. We have include data on G007-LK based PROTACs (Fig. S2D) in the revised manuscript.

> *(4) Throughout the manuscript, the authors need to do a better job at quantifying their results (i.e., the western blots and the IF). For example, the degradation of TNKS1/2 in Figure 1D is not overly convincing. Similarly, the IF data in Figure 3 needs to be quantified in some ways. Along the same lines, the effect of IWR1-POMA treatments on the proliferation of cells and organoids should be quantified using viability assays… There is also no indication of how many times these experiments were performed and whether the blots shown are representative experiments. The quantification should include all experiments.*

We have included quantification of the immunofluorescence images, colony formation data, and Western blots in the revised manuscript.

> ***Recommendations for the authors:***
>
> ***Reviewer #2 (Recommendations for the authors):***
>
> *(1) For clarity, can the authors use the official gene names, TNKS and TNKS2?*

We favor using TNKS1 and TNKS2 when referring to the protein for clarity and use TNKS for simplicity when referring to both proteins.

> *(2) Line 92: The authors refer to TNKS2 "induction" - it remains unclear what is meant by "induction".*

We have changed "without induction" to "under basal conditions".

> *(3) Can the authors please display molecular weight markers for Western blots throughout?*
>
> *(4) Line 144: The description "significantly more effectively" refers to Figure S5A, which shows a single, non-quantified Western blot. I don't think significance has been tested, and this statement should be reworded, or quantified aggregate data provided.*

We have added a Supplementary Information file showing molecular weight markers and quantification of Western blots.

> *(5) Line 226: "plateaued at a much lower level" - can this be expressed more quantitatively in the text?*

We have included more quantitative information on the FRAP results.

> *(6) Line 249: Can the authors repeat the cross-reference to Figure S7A here?*

We have repeated the cross-reference to the figures.

> *(7) Line 266: The description of the experiment using the GSPT1/2 degrader CC-90009 would benefit from a brief recap of the purpose as not every reader will be familiar with this common PROTAC off-target. This is a very thorough analysis, though, and commendable.*

We have added background information on GSPT1 degradation to the revised manuscript.

> *(8) Figure 1A: Can the number of repeats and the type of repeats be indicated, please?*
>
> *(9) Figure 2: Does n refer to biological or technical repeats?*
>
> *(10) Figure 5B, D: How many separate experiments are the data based on?*
>
> *(12) Figure S3D, S9A, D: number and types of repeats and the nature of the displayed data and error bars need to be included, please.*
>
> *(13) Figure S6B, S7B: I can see three data points, but it would still be helpful to state the number and type of repeats in the legend.*
>
> *(14) Figures S9A, S9D: There is value in showing the cumulative data from several repeats in the main figure (Figure 6, which currently is only qualitative) rather than the supplementary material.*
>
> *(15) Where single Western blots are shown, can the authors indicate how many experiments they are representative of?*

We have included the number of biological repeats for all data.

> *(11) Figure S2C: For most graphs, the main response of interest occurs at low compound concentrations. The y-axis scale does not always help the reader to appreciate the effects, as the response seems small against the magnitude of the hook effect. Interrupting the y-axis as in the final panel may help, with y-axis scales consistent over all panels in the figure.*

We have updated Fig. S2C to emphasize on the degradation efficacy.

> *(16) The authors may want to give further method details for some of their assays to facilitate replication of their experiments in the future. For example, the STF assay description is currently quite minimalistic. I assume the assay is fairly robust, though. Other details include cell media (general media details and specific additives and their*

> *concentrations in the 3D spheroid formation assay), etc. A general look at the methods section will likely be beneficial.*

We have updated the Methods section to provide more detailed experimental information.

> ***Reviewer #3 (Recommendations for the authors):***
>
> *(1) In Figure 2A, one of the most important findings of the manuscript is that IWR1-POMA induced promoted deeper suppression of beta-catenin-mediated transcription. This seems to be the case only at 3.2uM. Is it statistically significant? What are the data points on this graph? What are the error bars?*

We have included statistical analysis as Fig. S5G.

> *(2) On Figure 2C and 2D, do the authors know why the TNKS20M1054V mutant is much better at promoting signaling than the TNKS1-PD ? Is it expression levels?*

It is indeed interesting that TNKS2-M1054V promoted significantly stronger WNT signaling than TNKS1-PD. The basis for its strong scaffolding effect is unclear.

> *(3) In Figure 4C, the authors claim that when cells are treated with IWR1-POMA, AXIN1 is distributed diffusely throughout the cytoplasm. It appears that small punctae are visible.*

Quantitative analysis (Fig. 4F) suggest that the size of AXIN1 puncta upon IWR1-POMA is rather insignificant.

> *(4) Label on Figure 1D has a spelling error TNKS1/2.*

Corrected.

https://doi.org/10.7554/eLife.109052.2.sa0